CP violation and polarization effects in B-hadron decays

(diploma thesis submitted by Miroslav Sevelda)

Used literature is listed at the end of thesis and I declare no other literature has been used.

Contents

1 Introduction

The main goal of this thesis is the investigation of decays of beauty hadrons. After the introduction outlining the relevant ATLAS detector features the B-physics program at ATLAS here are summarized the principles of helicity formalism which is a useful tool for decay processes analysis.
The most important parts of the thesis are the parts discoursing of $\Lambda_b \to J/\psi\Lambda_0$ process analysis. This process is an important sample for Λ_b polarization measurements. The results presented are based on full inner detector simulations(GEANT program).
Next process studied is the $B_d \to J/\psi K^*$ which is a candidate for CP violation measurement. By means of an angular distribution it's possible to extract a parameter $\sin 2\beta$ that characterises CP violation. Results presented for this process are based on a particle level(PYTHIA program) simulations and discussed with regard for feasibility of $\sin 2\beta$ measurement.

2 General LHC and ATLAS features

Atlas is one of three high energy detectors which are being constructed at the Large Hadron Collider(LHC) at CERN. This collider should be able to accelerate protons up to nominal energy $7TeV$ per beam which gives $14TeV$ for collision in CM frame. Beside protons at LHC there will be accelerate also heavy ions(Pb). Basic parameters of LHC are shown in Table 1.

parameter	**proton mode**	**heavy ion mode**
Max.beam energy	14 TeV	2.76TeV/u
Initial luminosity	$10^{33}cm^{-2}s^{-1}$	$10^{33}cm^{-2}s^{-1}$
Nominal luminosity	$10^{34}cm^{-2}s^{-1}$	$10^{34}cm^{-2}s^{-1}$
Bunch spacing	25 ns	125 ns
Bunch lenght	7.5 cm	7.5 cm
dipole field	9 T	9 T

Table 1: Main LHC parameters

Physical processes proceeding during proton-proton collisions will be studied by force of two detectors:ATLAS and CMS. Main tasks of these experiments are in the searching for Higgs boson in mass range $80GeV < m_H < 1TeV$ and for new heavy particles predicted by some theories. There is of course a lot of other physical problems. For my thesis a B-physics tasks are very important. The most important problems of B-physics will be reviewed in the Chapter 4. As mentioned above, also heavy ions collisions will be studied at LHC. Main aim here are the study of quark-gluon plasma, its affections and conditions of quark-gluon plasma creation. Detector dedicated for these purposes is called ALICE.
In the thesis I focused myself on ATLAS detector. A rough technical description of ATLAS is presented in the Chapter 3. The most important part of the detector for my work, inner detector, is described in more detail there. The Chapter 5 contains the most important principles and results of helicity formalism. Exact explanation of this formalism is out of reach of this work. For more rigorous descrip-

tion of helicity formalism it is necessary to study literature cited in that chapter. My own work is presented in the following chapters 6,7. These parts contain concrete aplications of helicity formalism, i.e. determination of Λ_b^0 polarization based on the analysis of cascade decay $\Lambda_b^0 \to J/\psi(\to \mu^-\mu^+)\Lambda_0(\to p\pi)$ and determination of CKM(Cabbibo-Kobayashi-Maskawa) parameter $\sin 2\beta$ via analyzing of cascade decay $B_d^0 \to J/\psi(\to e^+e^-)K_0^*(\to K_0\pi_0)$. After some theoretical predictions and calculations there are results of Monte Carlo simulations of above cascade processes in ATLAS detector there.

3 The ATLAS detector

Whole ATLAS detector is based on cylindrical geometry and subdetectors are surrounding the 5 cm diameter beryllium beam pipe. Total dimension of ATLAS is dictated by the size of the muon spectrometer. The lenght of ATLAS is 41 meters and radius is about 11 meters. With respect to high collision frequency(bunch crossing each 25 ns, see Table 1) of LHC there must be very flexible and fast electonics there. ATLAS consists of several subdetectors with different functions in the particles identification processes.

3.1 The inner detector

The ATLAS inner detector is the innermost subdetector. It's contained inside the cylindrical space defined by radius R=115cm and $|z|$=345cm. The cavity is enclosed in solenoid with an axial magnetic field 2T. The inner detector provides continuous tracking with typically 36 points in transition radiation tracker and 7 space points in high precision high granularity semiconductor trackers for $|\eta| < 2.5$. Three types of detectors are implemented.
Pixel detectors are used in the nearest approach to the beam pipe.

They are contained on three layers at radii 4,11 and 14.2 centimeters. The nearest one is called vertexing layer or B-layer. It will enable a high precision vertex reconstruction for b-physics at initial low lumonosity mode. Layers consist of silicon pixels with size $50\mu m \times 300\mu m$. The point resolution is $\sigma(R \Leftrightarrow \phi) = 12\mu m$ in bending plane and $\sigma(z) = 60\mu m$ along the beam axis. The pixel system further includes 8 disc layers(4 on each side) covering $|\eta| < 2.5$ region. Their resolution is the same, $\sigma(R \Leftrightarrow \phi) = 12\mu m$ and $\sigma(z) = 60\mu m$.
Small angle stereo strip detectors are used as large area precision trackers. High precision is obtained in $R \Leftrightarrow \phi$ plane and a lower precision for non-bending plane. Four silicon layers are placed at radii $R = 30, 37.4, 44.7$ and 52 cm and 9 end-cap discs layers are placed at the endcap region. The strip size is $75\mu m \times 12cm$. The point resolution is $\sigma(R \Leftrightarrow \phi) = 16\mu m$ and $\sigma(z) = 580\mu m$.
The outermost subdetector is transition radiation tracker(TRT). TRT is situated at radii 62cm$< R <$110cm in barrel, and form of 18 wheel on each side of the end-cap part. TRT consist of large number of Kapton straws filled by magic mixture of gases $70\%Xe + 20\%CH_4 + 10\%CO_2$. Each staw is 4 mm diameter and it's resolution is $170\mu m$. Straws are solved as treshold detectors with two discrimination levels: 200 eV for usual ionisation and $5keV$ for transition radiation. The last treshold is very important for electron identification by TRT. Transition radiation created by electrons allows to identify them starting from $p_T > 0.5GeV$. The probability to identify electron is 92% for a hadron rejection factor of 25 in region $0.5GeV < p_T < 50GeV$.
The tracking requirements for b-physics involve also very low p_T tracks. The efficiency of a single electron reconstruction is better than 97% for $p_T > 1GeV$. The summary information about inner detector can be found in [34].

3.2 The electromagnetic calorimeter

The electromagnetic calorimeter uses lead absorber and liquid argon(LAr). The lead sheets are implemented in an accordion geometry, both for the barrel and the endcaps. The prototype measurement

of energy resolution is $\sigma(E)/E = 0.35\% \oplus 10\%\sqrt{E} \oplus 0.28\%/E$ (E given in GeV). A preshower detector is integrated in the calorimeter. A standalone electron identification probability is 75% for a rejection factor of 50 against hadrons and 10 against jets for $p_T > 2GeV$.
The electromagnetic calorimeter is capable of reconstructing neutral π mesons. The single π^0 simulation study showed that in the region of $2 < p_T < 5GeV$ π^0 can be reconstructed with the efficiency higher than 40% and with the mass resolution of $\sigma = 16MeV$.

3.3 The hadronic calorimeter

Inside the barrel toroid magnet there is a barrel hadron calorimeter made of iron and scintilator tiles. The energy resolution measured in a beam test for charged hadrons is $\sigma(E)/E = 47\%/\sqrt{E} \oplus 2.3\%$ (E in GeV). A study showed that the energy deposition in the last compartment of the calorimeter in depth, can be used for muon identification starting from $p_T \simeq 3GeV$. A hadron rejection factor of 50 at 80% muon efficiency was obtained.

3.4 The muon system

The air-core toroid system is capable of muon identification for $p_T > 5GeV$. Precision muon chambers allow standalone momentum resolution $\Delta p/p = 2\%$ in the range $20 < p_T < 200GeV$. At $p_T < 20GeV$ a standalone resolution is dominated by energy loss fluctuations in the calorimeter. The combined muon-inner detector tracking gives resolution $\Delta p/p = 1.5\%$ at $p_T = 20GeV$. The important role of muon system in triggering is discussed in next section.

3.5 The B-physics triggers

The three level ATLAS trigger is an optimal solution for meeting the requirement defined by:

- high rate(40 MHz) of LHC bunch crossings;
- high total cross section at 14 TeV;

- very low cross sections or branching ratios of new physics;
- limited amount of data that could be delivered to output media(10-100 MB/s)

The muon trigger system, based on dedicated fast response, high granularity detectors, can operate at 40 MHz through a full volume($|\eta| < 2.2$ and full azimuthal angle).The 6 GeV single muon trigger requires a coincidence with a 3/4 majority between two trigger detector double layer within a trigger road. The coincidence is required for the two projections(the bending and non-bending planes of muon system). A tight time coincidence $\Delta t < 20ns$ is also required in order to identify the bunch crossing.
Single muon trigger with $p_T > 6GeV$ enriches the $b\bar{b}$ event purity by a factor of 100. The statistics of $b\bar{b}$ events, which don't contain a muon among the signal particles or as a tag, is reduced by factor ~ 125 by LVL1 muon trigger. Another possible LVL1 trigger might be an isolated electromagnetic cluster with $p_T > 20GeV$. According to particle level simulation such a selection would however lead to reduction factor ~ 1000 for b-events containing electron.
After the confirmation of triggering muon at LVL2 by precision muon detectors, the next step is to search for features of certain b-physics processes.
The third level of trigger will provide full event reconstruction allowing more tight selection cuts and data reduction to the required 10-100 MB/s

4 B-physics and ATLAS

The main goals and problems which are going to be studied on ATLAS experiment have been completed in Atlas Technical Proposals and in Technical Design Report(TDR) of Inner Detector [33],[34].
The majority of B-physics measurements will be done during initial low luminosity($L = 10^{33}cm^{-2}s^{-1}$) LHC regime. Total cross section for $b\bar{b}$ production is about $\sigma_{b\bar{b}} = 500\mu b$, which gives 5×10^{12} $b\bar{b}$ pairs

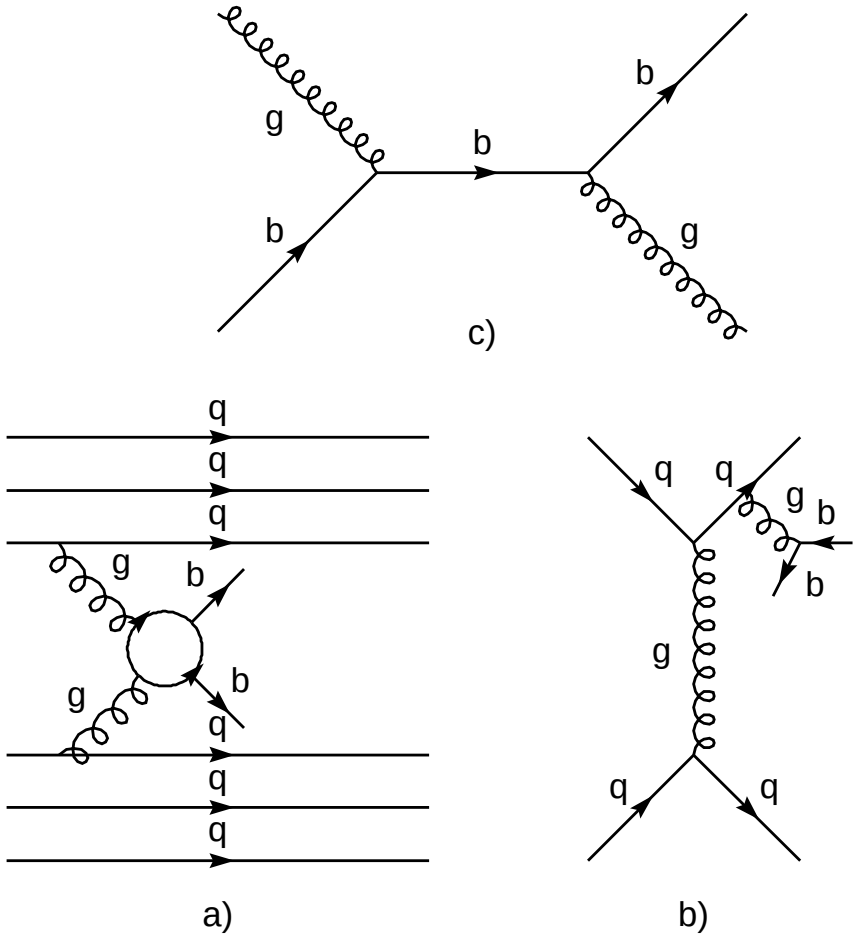

Figure 1: Three $b\bar{b}$ production mechanisms used in simulation. These are a)gluon-gluon fusion, b)gluon splitting in parton shower and c)flavor excitation(b-quarks from sea)

produced per year of run. Three dominant $b\bar{b}$ production mechanisms are included in our simulation program(see Fig.1).

Events containing pairs $b\bar{b}$ form about 1% of all events only. Events without $b\bar{b}$ pair form therefore a huge background. It has been shown that this background can be effectivelly reduced by LVL1 trigger conditions(i.e. event should contain have at least one muon with $p_T > 6GeV$ in active volume $|\eta| < 2.4$). These requirements are based on weak semileptonic decay of b-quark

$$b(\bar{b}) \rightarrow c(\bar{c}) + \mu^{+(-)} + \nu_\mu(\bar{\nu_\mu})$$

Large transverse momentum of muons can be a sign of heavy quark decay. About 40% of events with these muons contain heavy pair $b\bar{b}$. If we have a regard for these facts the total cross section for $b\bar{b}$ production is about $2\mu b$. Such cross section is sufficient for measurements of such phenomena as CP violation or B_s oscilations and for processes with small branching ratios. In searching for such phenomena LVL2 trigger plays an important role.

At nominal high luminosity regime the B-physics program will be based mainly on investigation of rare FCNC B-hadrons decays with small branchings (for example radiative decay $B_d \rightarrow K^*\gamma$). If we keep in mind the possibility of $B \Leftrightarrow \bar{B}$ mixing, we have to know flavor of decayed b-quark(i.e.b or $\bar{b}$) for measurement of CP violation or mixing of B_s. Few methods for this purpose(so called tagging methods) are under investigation. The easiest one is lepton charge method based on charge identification of lepton created in b-quark decay[21]. Another method is based on charge identification of pions coming from strong decays of highly excited B-hadrons(B^{**})[22]. The last method is based on charge measurement of a jet created along the primary b-quark direction[23]. The quality of above tags is shown in Table 2.

4.1 Measurement of CP violation

The first CP violation measurement has been done in the neutral kaon system and measured CP violating parameters were relativelly

Tag method	Tag efficiency	Wrong tag probability
lepton tag	0.2	0.22
π from B^{**}	0.26	0.28
jet charge	0.32	0.34

Table 2: b-quark tag methods quality.(Values taken from [19])

small. In B-meson system there is an evidence that we can expect more significant values of these parameters. The measurement of CP violation in B-meson systems can be expressed as measurement of three angles α, β, γ. These angles are the inner angles of the unitarity triangle(see below).
Charged current interactions of quarks have the form [31]

$$L = \frac{g}{2\sqrt{2}}(\bar{u}, \bar{c}, \bar{t})\gamma^{\mu}(1 \Leftrightarrow \gamma_5)V_{CKM}\begin{pmatrix} d \\ s \\ b \end{pmatrix} W_{\mu}^{+} + h.c. \tag{1}$$

where

$$V_{CKM} = \begin{pmatrix} V_{ud} & V_{us} & V_{ub} \\ V_{cd} & V_{cs} & V_{cb} \\ V_{td} & V_{ts} & V_{tb} \end{pmatrix}$$

is unitary quark mixing matrix($V_{CKM} = V_{CKM}^{\dagger}$). From unitarity we get three conditions

$$V_{ud}V_{ub}^{*} + V_{cd}V_{cb}^{*} + V_{td}V_{tb}^{*} = 0 \tag{2}$$

$$V_{us}V_{ub}^{*} + V_{cs}V_{cb}^{*} + V_{ts}V_{tb}^{*} = 0 \tag{3}$$

$$V_{ud}V_{us}^{*} + V_{cd}V_{cs}^{*} + V_{td}V_{ts}^{*} = 0 \tag{4}$$

Geometrically these equations form triangles in complex plane. The most important is triangle (2) and the CKM angles are defined as [30]

$$\alpha = arg(\Leftrightarrow\frac{V_{td}V_{tb}^{*}}{V_{ud}V_{ub}^{*}}), \quad \beta = arg(\Leftrightarrow\frac{V_{cb}V_{cd}^{*}}{V_{td}V_{tb}^{*}}), \quad \gamma = arg(\Leftrightarrow\frac{V_{ud}V_{ub}^{*}}{V_{cd}V_{cb}^{*}}) \tag{5}$$

It can be shown that matrix elements and decay widths of B-mesons are the functions of goniometrical functions of above angles. For example the decay width of the process $B_d \to K_s J/\psi$ is

$$\Gamma(\pm) \sim e^{-\Gamma t}(1 \pm \sin 2\beta \sin \Delta m t) \tag{6}$$

where $\pm$ stands for B_d and $\bar{B}_d$ respectively and Δm is the mass difference of B_d and $\bar{B}_d$ .If we define the asymmetry

$$A_{CP}(t) = \frac{\Gamma(+) \Leftrightarrow \Gamma(\Leftrightarrow)}{\Gamma(+) + \Gamma(\Leftrightarrow)} \tag{7}$$

we see that

$$A_{CP}(t) \sim \sin 2\beta \sin \Delta m t \tag{8}$$

We can measure the time-integrated asymmetry A_{CP}. Measured value of this asymmetry can be written in form [20]

$$A_{CP}^{obs} = D_{tag} D_{back}(D_{int} \sin 2\beta + A_P) \tag{9}$$

Here D_{tag} and D_{back} are dilution factors coming from wrong tags and from background effects, A_P is an additive factor coming from asymmetry in production and

$$D_{int} = \frac{\sin \Delta m t_0 + x_d \cos \Delta m t_0}{1 + x_d^2}$$

is the factor coming from time-integration. In this factor there $x_d = \frac{\Delta m}{\Gamma}$ is the factor of B_d-mixing and $x_d \sim 0.73$. Statistical error of $\sin 2\beta$ is therefore [20]

$$\delta(\sin 2\beta) = \frac{1}{D_{tag} D_{int} \sqrt{D_{back}} \sqrt{N}} \tag{10}$$

where N is the number of signal events. Analogically from asymmetry parameters of decays $B_d \to \pi^+\pi^-$ and $B_d \to J/\psi\Phi$ we can extract values of $\sin\alpha$ or $\sin\gamma$ respectively.

4.2 Beauty polarization

The beauty baryons polarization measurements give us important information about heavy quarks production mechanism and especially about its spin dependence. At ATLAS there will be some candidates for polarization measurements. The most feasible are polarization measurements of Λ_b and Ξ_b through their cascade decays $\Lambda_b \to J/\psi(l^-l^+)\Lambda_0(\pi_0 p)$ and $\Xi_b \to J/\psi(l^-l^+)\Lambda_0(\pi_0 p)$ respectively. More information about the former channel will be presented in next chapters as well as results of numerical simulations.

4.3 B_s-mixing

In Standard Model there are possibilities of neutral meson mixing(i.e.a neutral meson can be rearranged to its antiparticle). These processes can occur in higher orders of weak interactions in charged current sector. For example $B_s \Leftrightarrow \bar{B}_s$ mixing can be expressed by means of two Feynman diagrams(Fig.2).

Processes of this type generate non-equivalence of B-meson masses (i.e.$M(B_s) \neq M(\bar{B}_s)$). B_s-mixing is usually described by mixing parameter $x_s = \frac{\Delta m_B}{\Gamma_B}$. Standard Model prediction for this parameter is $12,9 < x_s < 26,1$. Mixing parameter can be determined by measurement of probability that the flavor of B_s at time $t = 0$ is the same as flavor of B_s at time $t = t_0$.

4.4 Rare B-decays

The main aim here is in searching for B-decays caused by flavor changing neutral currents(FCNC). These processes can give us indications of physics beyond Standard Model. Examples of this type are leptonic decays $B_s \to \mu^+\mu^-$,$B_d \to \mu^+\mu^-$ or radiative decays $B_d \to \rho\gamma$ and $B_d \to K^*\gamma$. The last two decays can be also used for precise determination of ratio $|V_{ts}|/|V_{td}|$.

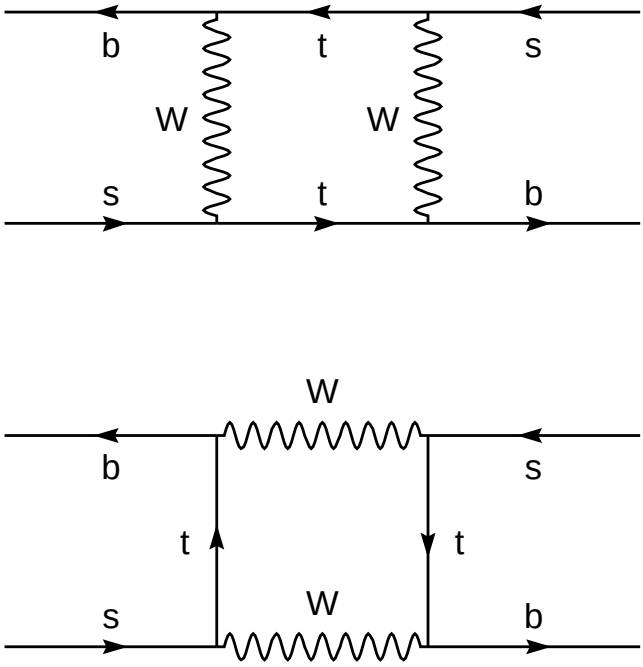

Figure 2: Feynmann diagrams of $B_s - \bar{B}_s$ mixing

5 Main principles and results of helicity formalism

In many cases in physics we have to study the angular distributions of secondary particles coming from decay of another particle. For this purpose the helicity formalism has been developed. In contrast to the other methods the helicity formalism is relatively simple and very flexible. Using of helicity formalism we can keep clear of usual problems connected with Lorentz transformations between coordinate systems thanks to Lorentz invariance of helicity operator. This chapter gives main results and principles only. For more details see [10] and [5].

Helicity of a particle is defined as a projection of particle's spin into the direction defined by its momentum, i.e.

$$\lambda = \vec{s} \cdot \frac{\vec{p}}{|\vec{p}|} \tag{11}$$

In case of particle at rest helicity is equivalent to spin projection into chosen axis.

Let's consider a particle with spin $\vec{s}$ at rest now. This particle can be described by plane wave state vector

$$|\vec{p} = 0, \vec{s}, \lambda > \tag{12}$$

It's apparent that all states of this particle in motion along z axis, i.e. $\vec{p}_z \neq 0$ can be created by Lorentz transformation along z-axis

$$|\vec{p}_z, \vec{s}, \lambda > = \hat{L}(\vec{p}_z)|\vec{p} = 0, \vec{s}, \lambda > \tag{13}$$

In the case of arbitrary direction of motion we can generate the state vector by aplication of Lorentz transformation and rotation to axis of motion

$$|\vec{p}, \vec{s}, \lambda > = \hat{R}(\alpha\beta\gamma)\hat{L}(\vec{p}_z)|\vec{p} = 0, \vec{s}, \lambda > \tag{14}$$

or

$$|\vec{p}, \vec{s}, \lambda > = \hat{L}(\vec{p})\hat{R}(\alpha\beta\gamma)|\vec{p} = 0, \vec{s}, \lambda > \tag{15}$$

where α, β, γ are usual Euler angles. For description of system of two particles, we can write

$$|\vec{p}_1, \vec{s}_1, \lambda_1; \vec{p}_2, \vec{s}_2, \lambda_2 >= |\vec{p}_1, \vec{s}_1, \lambda_1 > \otimes |\vec{p}_2, \vec{s}_2, \lambda_2 >$$

If we describe a two-particle system in CMS frame, this vector can be rewritten to $|p\theta\phi\lambda_1\lambda_2 >$, where θ and ϕ are polar and azimuthal angles. It can be shown that these state vectors form complete system of vectors. Of course there exist another base formed by vectors $|pJM\lambda_1\lambda_2 >$ where J and M is total angular moment and its projection of particle system. Relation between these two basis can be written as

$$|p\theta\phi\lambda_1\lambda_2 >= \sum_{J,M} \sqrt{\frac{2J+1}{4\pi}} \mathcal{D}^J_{M\lambda_1-\lambda_2}(\phi\theta\phi)|pJM\lambda_1\lambda_2 > \tag{16}$$

where $\mathcal{D}$ are Wigner rotation functions with normalization

$$\int_0^{2\pi}\int_0^{\pi}\int_0^{\pi} \mathcal{D}^J_{MN}\mathcal{D}^{J'}_{M'N'} \cos\beta d\alpha d\beta d\gamma = \frac{8\pi}{2J+1}\delta_{MM'}\delta_{NN'}\delta_{JJ'} \tag{17}$$

It's useful to factorize out the momenta and then state vectors can be rewritten as

$$|p\theta\phi\lambda_1\lambda_2 >= (2\pi)^3(\frac{4\sqrt{s}}{p})^{1/2}|\theta\phi\lambda_1\lambda_2 > |p > \tag{18}$$

$$|pJM\lambda_1\lambda_2 >= (2\pi)^3(\frac{4\sqrt{s}}{p})^{1/2}|JM\lambda_1\lambda_2 > |p > \tag{19}$$

where $\sqrt{s}$ is total energy of two-particle system in CM-frame. For both state vectors we can write down the normalization conditions

$$< \theta'\phi'\lambda_1'\lambda_2'|\theta\phi\lambda_1\lambda_2 >= \delta(\cos\theta' \Leftrightarrow \cos\theta)\delta(\phi' \Leftrightarrow \phi)\delta_{\lambda_1'\lambda_1}\delta_{\lambda_2'\lambda_2} \tag{20}$$

$$< p'J'M'\lambda_1'\lambda_2'|pJM\lambda_1\lambda_2 >= \delta^3(p' \Leftrightarrow p)\delta_{M'M}\delta_{J'J}\delta_{\lambda_2'\lambda_2}\delta_{\lambda_1'\lambda_1} \tag{21}$$

$$< p|p^{'} >= \delta^4(p \Leftrightarrow p^{'}) \tag{22}$$

and for scalar product of two basis can be found relation

$$< JM\lambda_1^{'}\lambda_2^{'}|\theta\phi\lambda_1\lambda_2 >= \sqrt{\frac{2J+1}{4\pi}}\delta_{\lambda_2^{'}\lambda_2}\delta_{\lambda_1^{'}\lambda_1}\mathcal{D}^J_{M\lambda_1-\lambda_2}(\phi\theta \Leftrightarrow \phi) \tag{23}$$

With the help of above equations is easy to write down the angular distribution for process $a+b \to c+d$. For T-operator matrix element we get

$$< f|T|i >=< cd|T|ab >= (2\pi)^6\sqrt{\frac{2s}{p_i p_f}} < \theta\phi\lambda_c\lambda_d|T|00\lambda_a\lambda_b > \tag{24}$$

where $|p_i| = |p_a| = |p_b|$ and $|p_f| = |p_c| = |p_d|$ are initial and final momenta of particles in CM-frame. If we use relation of completeness (i.e.$\sum |JM\lambda_a\lambda_b >< JM\lambda_a\lambda_b| = 1$ and $\sum |JM\lambda_c\lambda_d >< JM\lambda_c\lambda_d| = 1$), we can get the angular distribution in form

$$\frac{d\sigma}{d\Omega} = |< f|T|i >|^2 = \frac{4s(2\pi)^4}{p_i p_f}\sum_{\lambda_i,\lambda_f,\lambda_i^{'},\lambda_f^{'}}(\frac{2J+1}{4\pi})^2\mathcal{D}^{J*}_{\lambda_i\lambda_f}\mathcal{D}^J_{\lambda_i^{'}\lambda_f^{'}}T_{\lambda_a\lambda_b\lambda_c\lambda_d} \tag{25}$$

Analogically for decay $a \to b + c$ we find

$$\frac{d\sigma}{d\Omega} = \sum_{\lambda_f,\lambda_f^{'},M,M^{'}}\frac{2J+1}{4\pi}\mathcal{D}^{J*}_{M\lambda_f}\mathcal{D}^J_{M^{'}\lambda_f^{'}}T_{\lambda_a\lambda_b\lambda_c} \tag{26}$$

In above equations $T_{\lambda_a\lambda_b\lambda_c\lambda_d} =< \lambda_c\lambda_d|T|\lambda_a\lambda_b >$, $T_{\lambda_a\lambda_b\lambda_c} =< \lambda_b\lambda_c|T|\lambda_a >$ are helicity amplitudes and $\lambda_i = \lambda_a \Leftrightarrow \lambda_b$, $\lambda_f = \lambda_c \Leftrightarrow \lambda_d$. This method can be easily extended to cascade decays, i.e. processes of type $a \to b(\to p+q) + c(\to r+s)$. More details can be found in references[5],[10].

If we study processe that conserve intrinsic parity, helicity amplitudes aren't independent. For example parity conservation in process $a + b \to c + d$ leads to conditions

$$< \lambda_c\lambda_d|T|\lambda_a\lambda_b >= \eta_a\eta_b\eta_c\eta_d(\Leftrightarrow 1)^{s_c+s_d-s_a-s_b} < \Leftrightarrow\lambda_c \Leftrightarrow\lambda_d|T|\Leftrightarrow\lambda_a \Leftrightarrow\lambda_b > \tag{27}$$

For decay of a particle a, $a \to b + c$ we could find

$$< \lambda_b \lambda_c | T | \lambda_a >= \eta_a \eta_b \eta_c (\Leftrightarrow 1)^{s_b + s_c - J} < \Leftrightarrow \lambda_b \Leftrightarrow \lambda_c | T | \lambda_a > \tag{28}$$

where $\eta_a, \eta_b, \eta_c, \eta_d$ are intrinsic parities of particles a, b, c, d with spins s_a, s_b, s_c, s_d.

6 Λ_b polarization

As it has been said above ATLAS experiment will be able to measure polarization of beauty baryon. Polarization(or polarization asymmetry) of a particle is defined as

$$P = \frac{|A_m|^2 \Leftrightarrow |A_{-m}|^2}{|A_m|^2 + |A_{-m}|^2} \tag{29}$$

where A_m and A_{-m} are matrix elements corresponding to decay of particle with spin projection m and $\Leftrightarrow m$ into chosen axis. In case of Λ_b is $m = \frac{1}{2}$. If we know production mechanism of Λ_b we can define polarization as [17]

$$P = \frac{\rho_{\frac{1}{2}\frac{1}{2}} \Leftrightarrow \rho_{-\frac{1}{2}-\frac{1}{2}}}{Tr(\rho)} \tag{30}$$

where ρ_{ij} are elements of spin density matrix of Λ_b. In the range of low transverse momenta of Λ_b baryon a significant values of polarization are expected. The main reasons for this assumption come from Λ_0 polarization measurements, where Λ_0's are produced in pp or $p\bar{p}$ collisions. There is a close analogy between Λ_b and Λ_0 production mechanisms because in both cases a heavier quark unpresent in basic configuration ought to be created [17]. QCD calculations including gluon distribution functions in proton give for polarized matrix element [32]

$$A_{pol} \sim \frac{x x_F [(x_F \Leftrightarrow 4/9)^2 \Leftrightarrow 7/81]}{1 + x_F^2} \otimes \Omega(M, P_T) \tag{31}$$

where

$$\Omega(M, P_T) = \frac{3MP_T}{P_T^2 + M^2} \tag{32}$$

and $x_F = u/sy, \quad x = t/s(1 \Leftrightarrow x_F)$. Parameters s,t,u are usual Mandelstam variables and y is a scalling factor.
Here M and P_T are mass and transverse momentum(transverse to the initial proton beam direction) of baryon(Λ_b here). Function $\Omega(M, P_T)$ is shown in Fig.3 as well as its shape for fixed value $M = M(\Lambda_b) = 5.678GeV$. Next Fig.4 also shows distribution of transverse momentum of Λ_b.

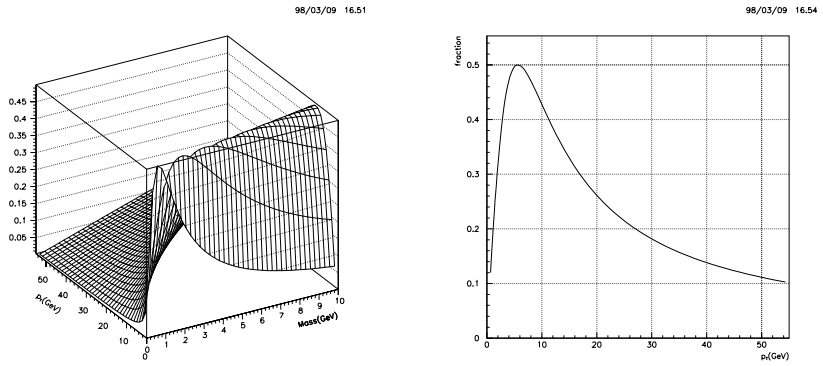

Figure 3: P_T dependent part of polarized matrix element(function $\Omega(M, P_T)$). Left 3D-plot shows full dependence of Ω on p_T and M and the right one shows this dependence for fixed $M = M(\Lambda_b) = 5.678GeV$

6.1 Method of polarization determination

Polarization of Λ_b can be determined from angular distribution of cascade decay $\Lambda_b \to J/\psi(\to \mu^-\mu^+)\Lambda_0(\to p\pi)$. The distribution of angle between the beauty baryon decay analyzer and the production analyzer is

$$w(\theta) = \frac{1}{2}(1 + \alpha_b P_b \cos\theta) \tag{33}$$

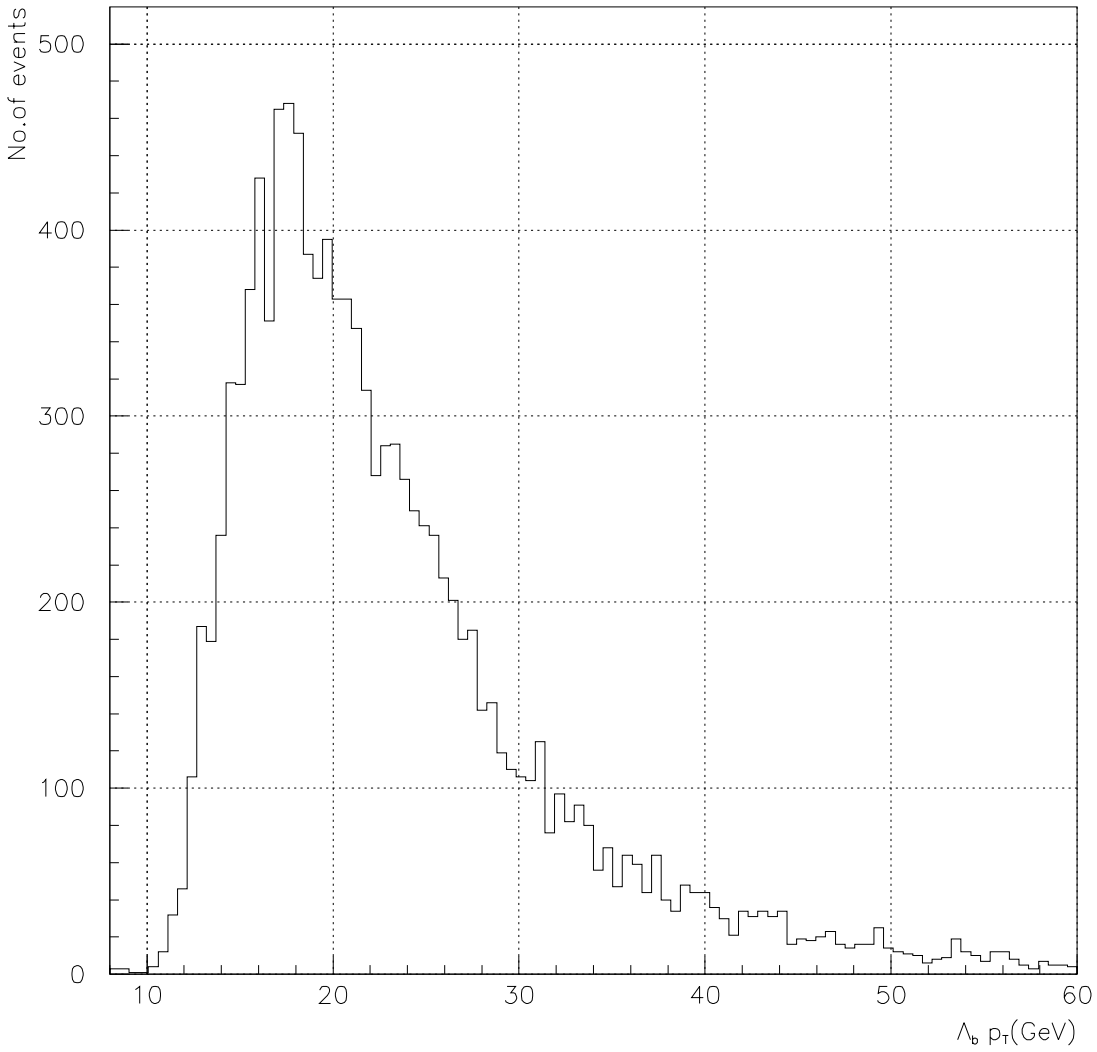

Figure 4: Distribution of Λ_b transverse momentum for unpolarized Λ_b

where α_b is the asymmetry parameter and P_b is a projection of polarization vector to the production analyzer [1] . The direction of the production analyzer is the same as the direction of production plane normal vector $\vec{n} = \frac{\vec{p}_{in} \times \vec{p}_b}{|\vec{p}_{in} \times \vec{p}_b|}$ where $\vec{p_{in}}$ is initial proton momentum and $\vec{p}_b$ is Λ_b momentum. Because the asymmetry parameter is still unknown as well as a polarization, its necessary to measure these parameters simultaneously. For this purpose it is profitable to use the full angular distribution of cascade decay of Λ_b. From the point of view of helicity formalism this cascade decay can be described by four helicity amplitudes(parity nonconservation process)

$$a_+ = T_{1/20}, \quad a_- = T_{-1/20}, \quad b_+ = T_{-1/21}, \quad b_- = T_{1/2-1}$$

These amplitudes have to satisfy the normalization condition

$$|a_+|^2 + |a_-|^2 + |b_+|^2 + |b_-|^2 = 1 \tag{34}$$

By means of the amplitudes we can express asymmetry parameter as

$$\alpha_b = |a_+|^2 \Leftrightarrow |a_-|^2 + |b_+|^2 \Leftrightarrow |b_-|^2 \tag{35}$$

If we use the methods described in Chapter 5, we can get the cascade decay angular distribution [1],[3]

$$W(\Omega, \Omega_1, \Omega_2) = \sum_{i=0}^{i=19} f_{1i} f_{2i}(P_b, \lambda_b) F_i(\Omega, \Omega_1, \Omega_2) \tag{36}$$

where functions f_{1i}, f_{2i} and F_i are listed in Table 8 in Appendix.

$\Omega = (\theta, \phi)$ are the polar and the azimuthal angles of Λ_0 momentum in the Λ_b rest frame with the axis $z \| \vec{n}$. Other axes are arbitrary because of parity invariance of Λ_b production process which guarantees the ϕ-independence. $\Omega_1 = (\theta_1, \phi_1)$ are the angles of proton momentum in Λ_0 rest frame with axes $z_1 \| \vec{p}_{\Lambda_0}$, $y_1 \| \vec{n} \times \vec{p}_{\Lambda_0}$ and $\Omega_2 = (\theta_2, \phi_2)$ are the angles of the momentum of one lepton in J/ψ rest frame with axes $z_2 \| \vec{p}_{J/\psi}$, $y_2 \| \vec{n} \times \vec{p}_{J/\psi}$.

There are 7 unknown independent parameters in this angular distribution. Six of them are determined by helicity amplitudes

$$a_+ = |a_+| e^{i\alpha_+}, a_- = |a_-| e^{i\alpha_-}, b_+ = |b_+| e^{i\beta_+}, b_- = |b_-| e^{i\beta_-} \tag{37}$$

and the seventh one is the polarization projection P_b. These parameters can be determined from angular distribution by momentum method. This method is based on orthogonality of F_i. So if we have

$$\int F_i(\Omega,\Omega_1,\Omega_2)F_j(\Omega,\Omega_1,\Omega_2)d\Omega d\Omega_1 d\Omega_2 \sim \delta_{ij}$$

we can determine the product $f_{1k}f_{2k}$ as

$$< F_k >= \frac{\int\int\int W(\Omega,\Omega_1,\Omega_2)F_k(\Omega,\Omega_1,\Omega_2)d\Omega d\Omega_1 d\Omega_2}{\int\int\int W(\Omega,\Omega_1,\Omega_2)d\Omega d\Omega_1 d\Omega_2} \qquad (38)$$

These moments are observables which can be determined from experiment. Then if we calculate them we can get a system of equations for 7 independent parameters. With help of weighted least-square method we can calculate the errors of these parameters. For this method the error of polarization falls to range $\delta(P_b) \in \frac{1}{N_b}(2.5, 4.7)$ where N_b is the number of Λ_b events.
Beauty baryons Λ_b can be produced directly or via the decays of heavier states in strong processes

$$\Sigma_b \to \Lambda_b\pi_0$$

$$\Sigma_b^* \to \Lambda_b\pi_0$$

For observed value of polarization P_{obs} we then get

$$P_{obs} = \frac{BR(\Lambda_b) + \sum_i(\frac{-1}{3}BR(\Sigma_{bi})P_{\Sigma_{bi}} \Leftrightarrow \frac{1}{3}BR(\Sigma_{bi}^*)P_{\Sigma_{bi}^*})}{BR(\Lambda_b) + \sum_i(BR(\Sigma_{bi}) + BR(\Sigma_{bi}^*))} \qquad (39)$$

where the branching ratios are $BR(\Lambda_b) = BR(b \to \Lambda_b)$, $BR(\Sigma_b) = BR(b \to \Sigma_b)$ and the sum runs over charged and neutral Σ_b baryons.

6.2 Λ_b decay chain identification and reconstruction

For purpose of $\Lambda_b \to J/\psi(\to \mu^-\mu^+)\Lambda_0(\to p\pi)$ decay analysis a sample of about 33 000 particle level events of type $pp \to b\Lambda_b X \to \Lambda_b(\Lambda_0 J/\psi)$ has been generated. This channel can be self-triggered if we require LVL1 trigger condition, i.e. one muon with $p_T > 6GeV$ in the volume $|\eta| < 2.5$. At the Pythia(B-Atgen) level the event has been accepted if

- transverse momentum of p and π, $p_T > 0.5GeV$ in $|\eta| < 2.5$;
- transverse momentum of muons from J/ψ decay, $p_T > 3GeV$ and $p_T > 6GeV$ in $|\eta| < 2.5$;

I generated these events with unpolarized Λ_b. Polarization can be included by weighting the unpolarized events according to certain models. Particle level events are stored in ZEBRA banks. These banks are read by detector simulation code(DICE based on GEANT) [37]which performs **the full inner detector simulation**. As an output DICE retrieves ZEBRA banks containing digitized information (full inner detector response). In a final phase the reconstruction of digitized events is performed by ATLAS reconstruction package XKALMAN[35], [36] followed by dedicated vertex fitting program adopted from CDF(This fit program is based on the parametric least square algorithm and fit quality is characterized by χ^2 per degree of freedom(ndof)). After reconstruction we get banks containing reconstructed tracks parameters(in form of five dimensional helix vector and 5×5 covariance matrix).
Basic principle of Λ_b reconstruction is as follows. Firstly J/ψ is reconstructed from two tracks with opposite charge. We want to reconstruct $J/\psi \rightarrow \mu(p_T > 6)\mu(p_T > 3)$ and therefore we look for $track(p_T > 3) \oplus \mu(p_T > 6)$ combinations. Based on ATLAS μ-trigger studies we suppose that muon with $p_T > 6GeV$ is identified in muon system with probability 0.85 and with negligible hadron contribution. Muon with $3 < p_T < 5GeV$ will be identified in last compartment of tile calorimeter. Test beam analyses showed high efficiencies(~ 0.9) with large hadron rejection(~ 90). It means that if $track(p_T > 3)$ is a hadron this combination is used with probability ≈ 0.011. Tracks with these properties are fitted to common vertex. Invariant mass distribution of succesfully fitted tracks($\chi^2/ndof < 20$) is shown in Fig.5. As a J/ψ candidates can be assigned these combination with invariant mass $M_{track(p_T>3)\oplus\mu(p_T>6)} \in < \Leftrightarrow 3\sigma, 3\sigma >$ around nominal J/ψ mass(here $\sigma = 39MeV$).This invariant mass is shown in Fig.6.
When J/ψ candidates are present we look for Λ_0 candidates. The finding algorithm is an analog of the J/ψ one. Here are combined

two oppositely charged tracks with minimal transverse momentum for reconstruction($p_T > 0.5GeV$). In addition we require production radius of both tracks to be within $< 1,44 > cm$. The lower bound reduces background from Λ_0's coming directly from the primary vertex and the upper one is for precise Λ_0 reconstruction.(For better resolution we need hits from silicon SCT layers). Tracks are fitted to the common vertex with assumption that track with higher p_T is a proton(leading particle effect). Invariant mass distribution of tracks after succesfull common vertex fit($\chi^2/ndof < 6$) is shown in Fig.7. As a Λ_0 candidates has been assigned those combinations with invariant mass $M_{track \oplus track} \in < \Leftrightarrow 3\sigma, 3\sigma >$ around nominal Λ_0 mass.(Here $\sigma = 2.5MeV$). Invariant mass of fitted Λ_0 candidates is shown in Fig.8. The efficiency of Λ_0 reconstruction as a function of Λ_0's transverse momentum and decay radius is shown in Fig.9 and Fig.10. The reconstruction efficiency is defined as the ratio of the number of events which pass all fitting cuts(see text) to the total number of Monte Carlo events having Λ_0 decay radius between 1 and 44 cm and proper time of Λ_b greater than $0.5ps$. Finally if we have J/ψ and Λ_0 candidates a global Λ_b fit is performed for $J/\psi \oplus \Lambda_0$ system. Here vertex and mass constraints are applied to both J/ψ and Λ_0 vertices. Vertex constraint means that Λ_0 momentum vector was constrained to point to J/ψ vertex and fitted Λ_b momentum vector to the primary vertex. Invariant mass distribution of $J/\psi \oplus \Lambda_0$ after succesful global common vertex fit is shown in Fig.11. As a Λ_b candidates we assigned combinations with invariant mass $M_{J/\psi \oplus \Lambda_0} \in < \Leftrightarrow 3\sigma, 3\sigma >$ around nominal Λ_b mass.(Here $\sigma = 22MeV$). This invariant mass distribution is shown in Fig.12. If there is more than one $J/\psi, \Lambda_0$ and Λ_b candidate I took only one with minimal mass residual (i.e.those with $M_{fit} \Leftrightarrow M_{nominal} = min$).

Other reconstruction characteristics of Λ_b i.e. Λ_b proper time residuals and Λ_b decay radius residuals are shown in Fig.13 and Fig.14. Overall information about $\Lambda_b \rightarrow J/\psi\Lambda_0$ reconstruction are listed in Table 10.(In Appendix) [p]

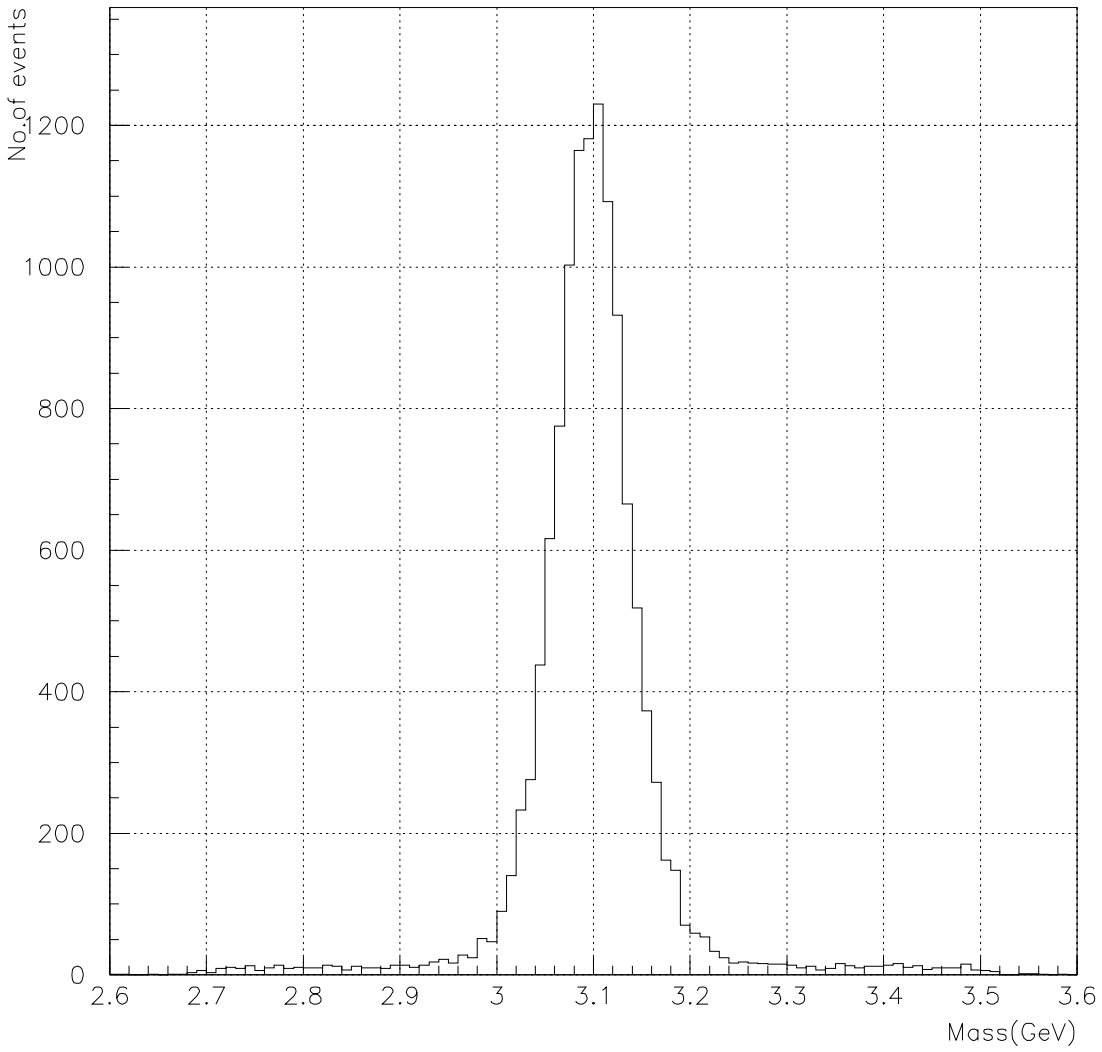

Figure 5: $track(p_T > 3) \oplus \mu(p_T > 6)$ invariant mass after common vertex fit(J/ψ) This is invariant mass of $track(p_T > 3GeV) \oplus \mu(p_T > 6GeV)$ with positive common vertex fit ($\chi^2/ndof < 20$)

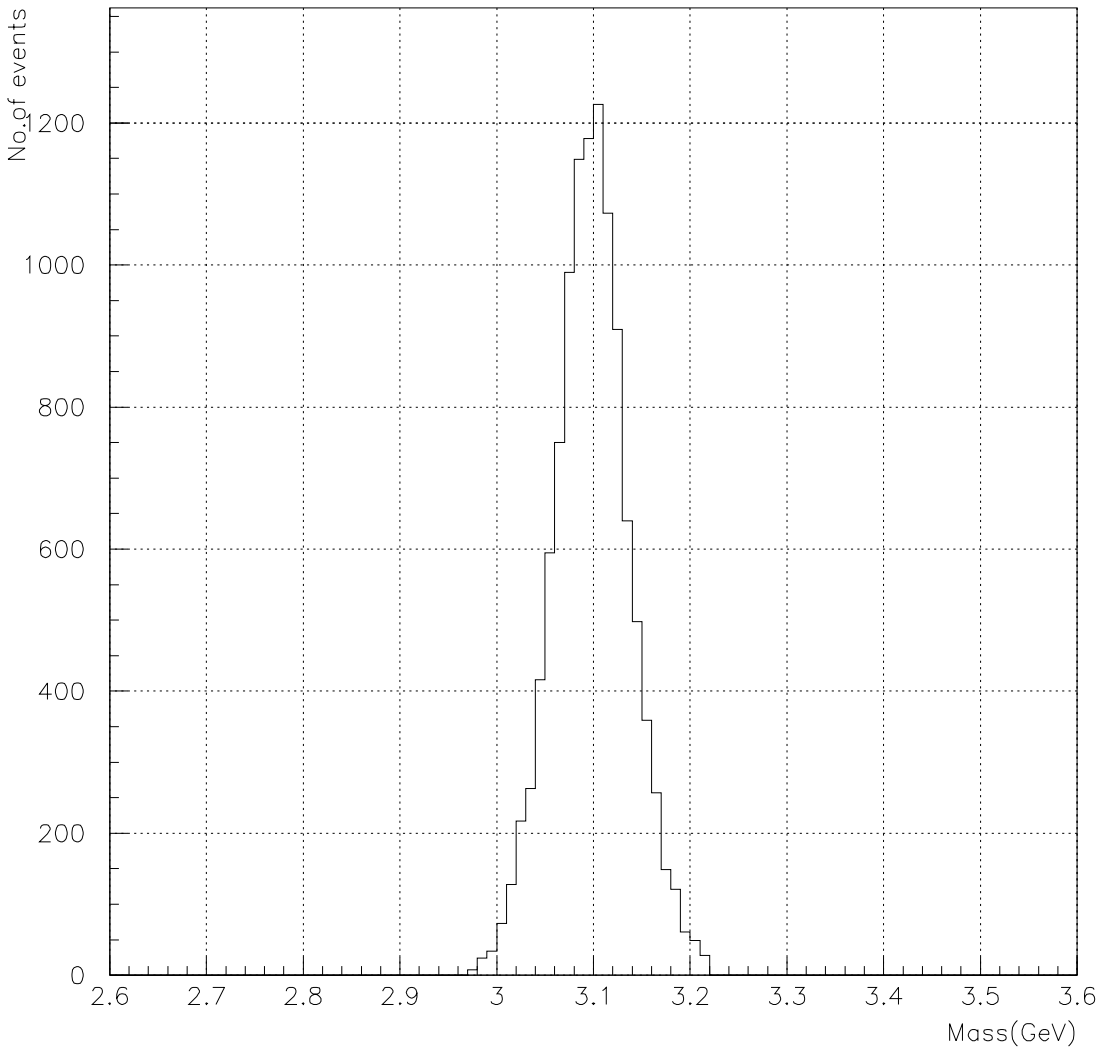

Figure 6: Fitted J/ψ invariant mass distribution. Gaussian fit to the peak gives $\sigma = 39.3 MeV$.

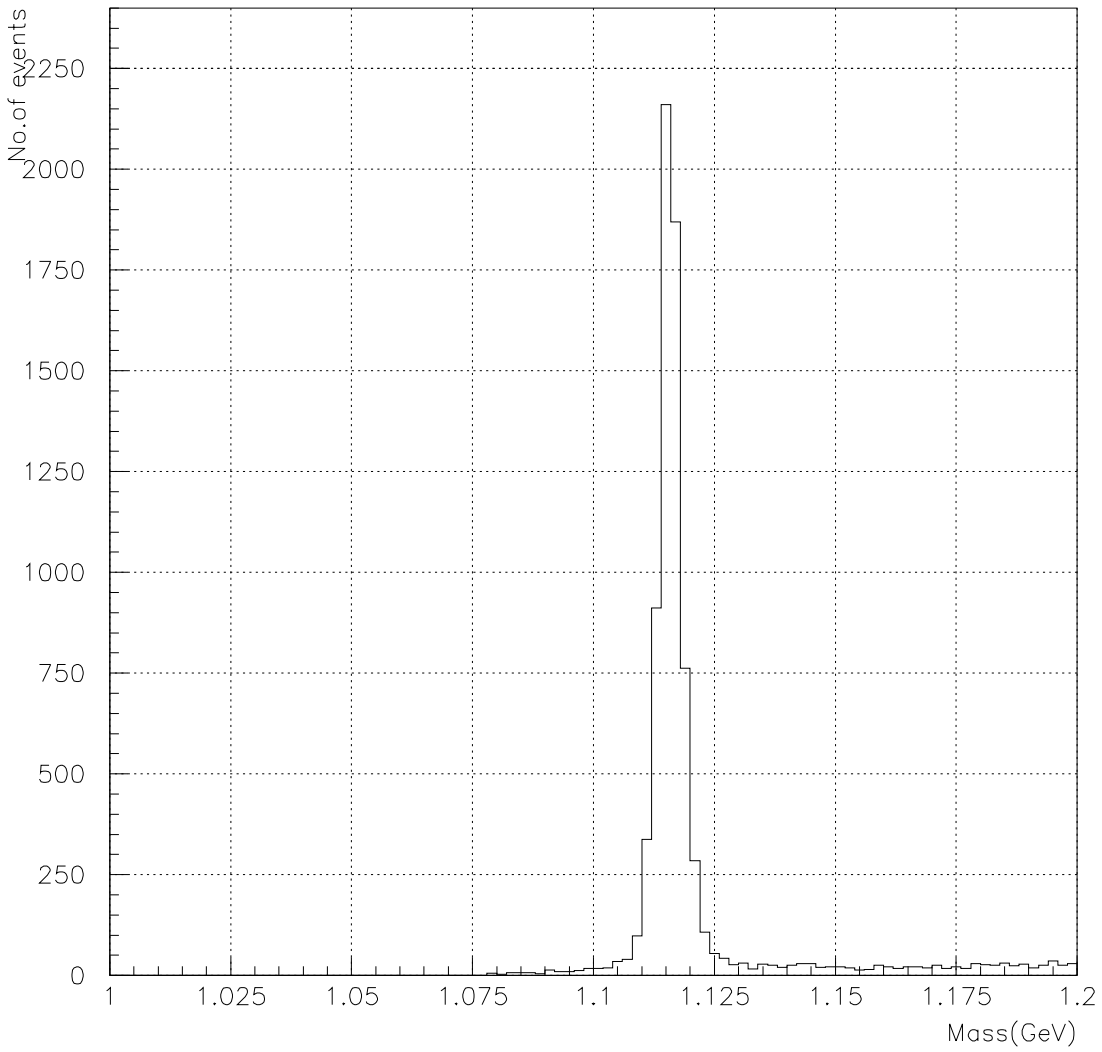

Figure 7: $track(p_T > 0.5) \oplus track(p_T > 0.5)$ invariant mass distribution after common vertex fit(Λ_0) This histogram shows invariant mass of combinations $track(p_T > 0.5GeV) \oplus track(p_T > 0.5GeV)$ with positive common vertex fit($\chi^2/ndof < 6$) and with creation radius within $< 1,44 > cm$ in transverse plane

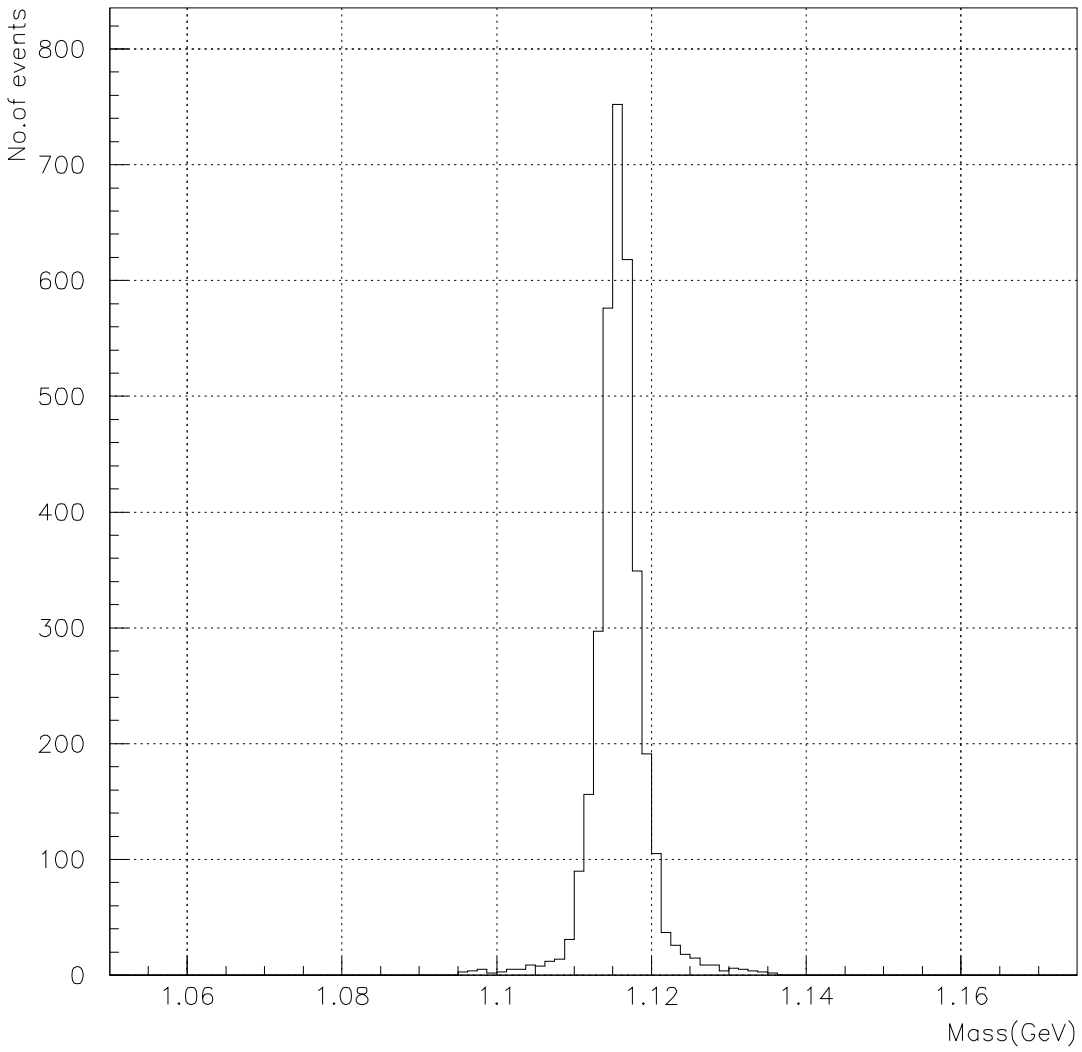

Figure 8: Fitted Λ_0 invariant mass distribution. Gaussian fit to the peak gives $\sigma = 2.5MeV$

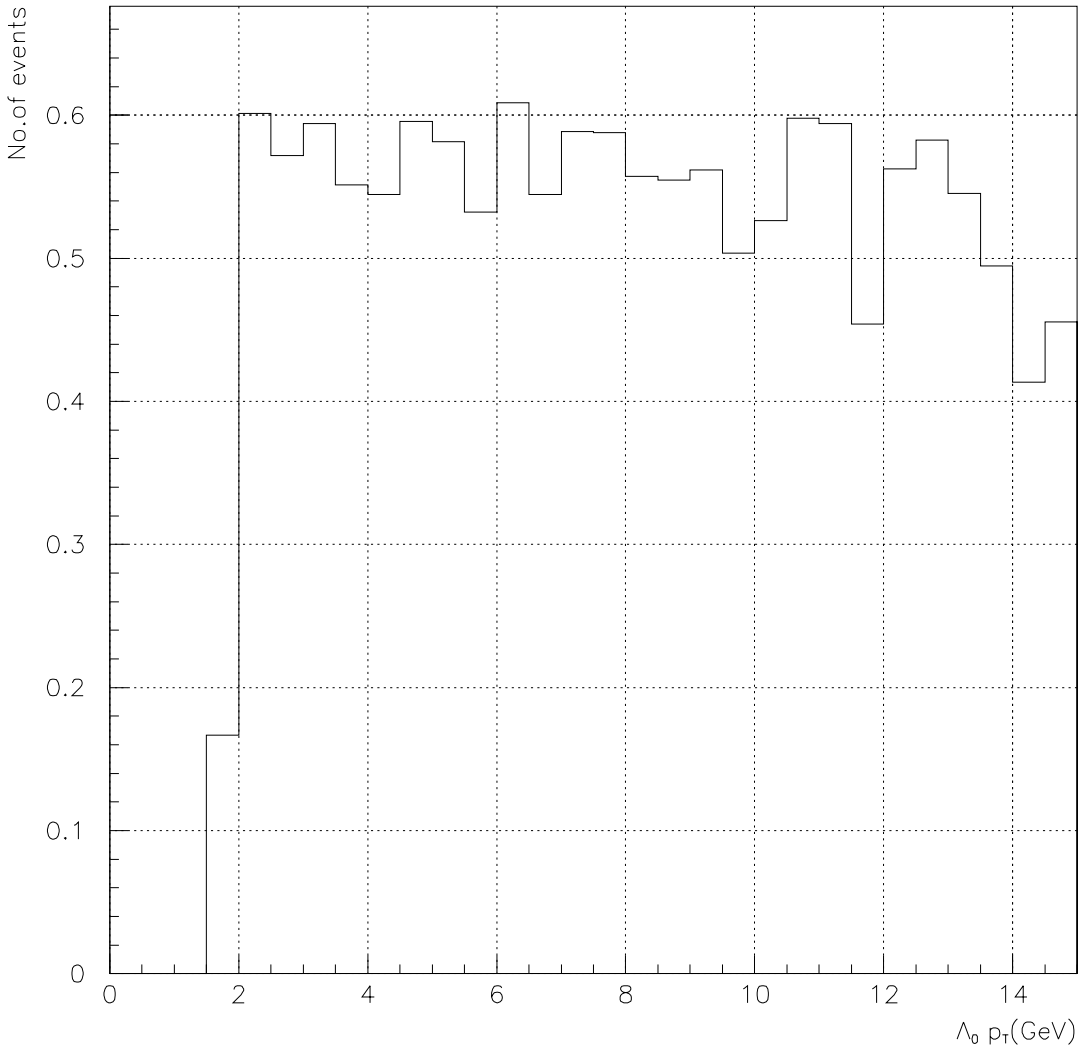

Figure 9: Λ_0 reconstruction efficiency as a function of $p_T(\Lambda_0)$

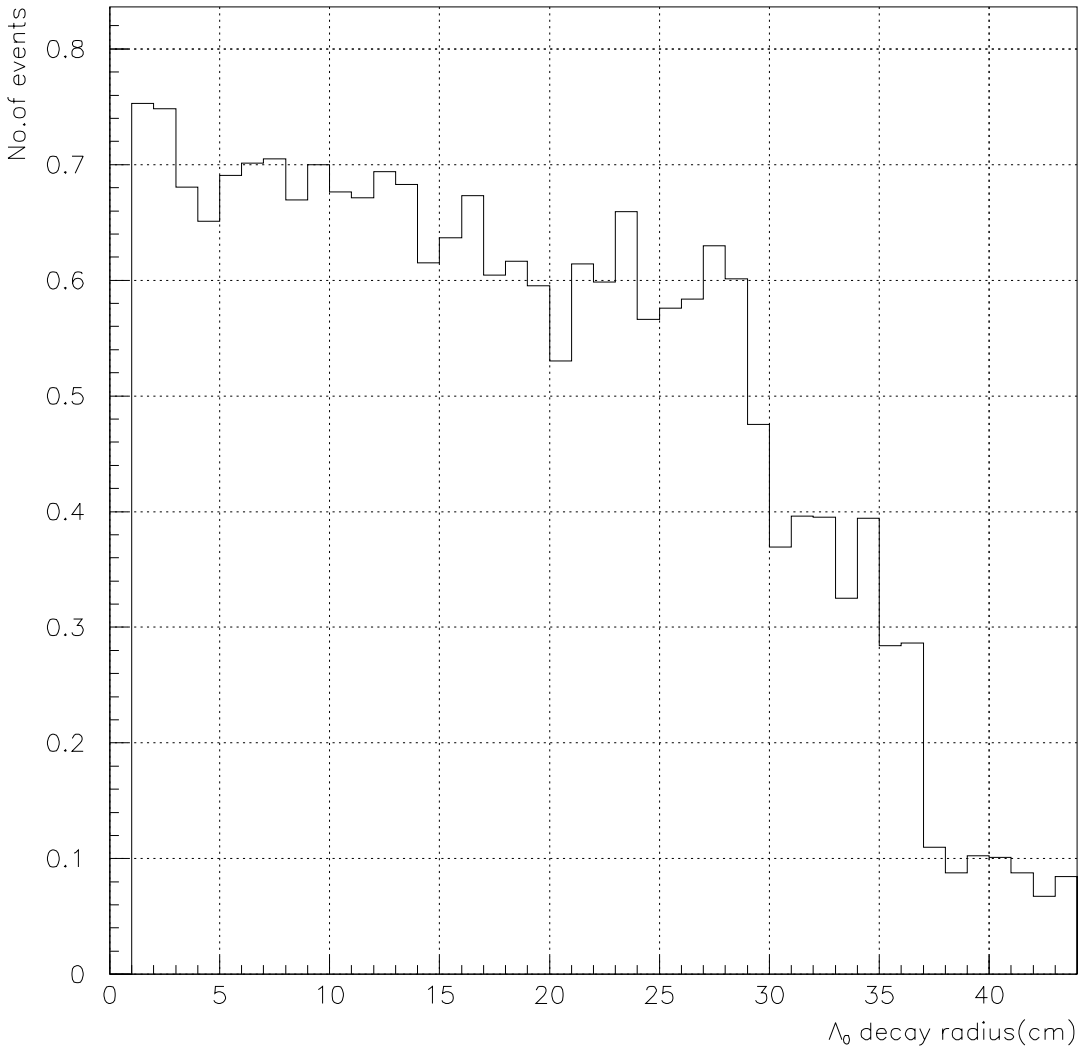

Figure 10: Λ_0 reconstruction efficiency as a function of decay radius of Λ_0

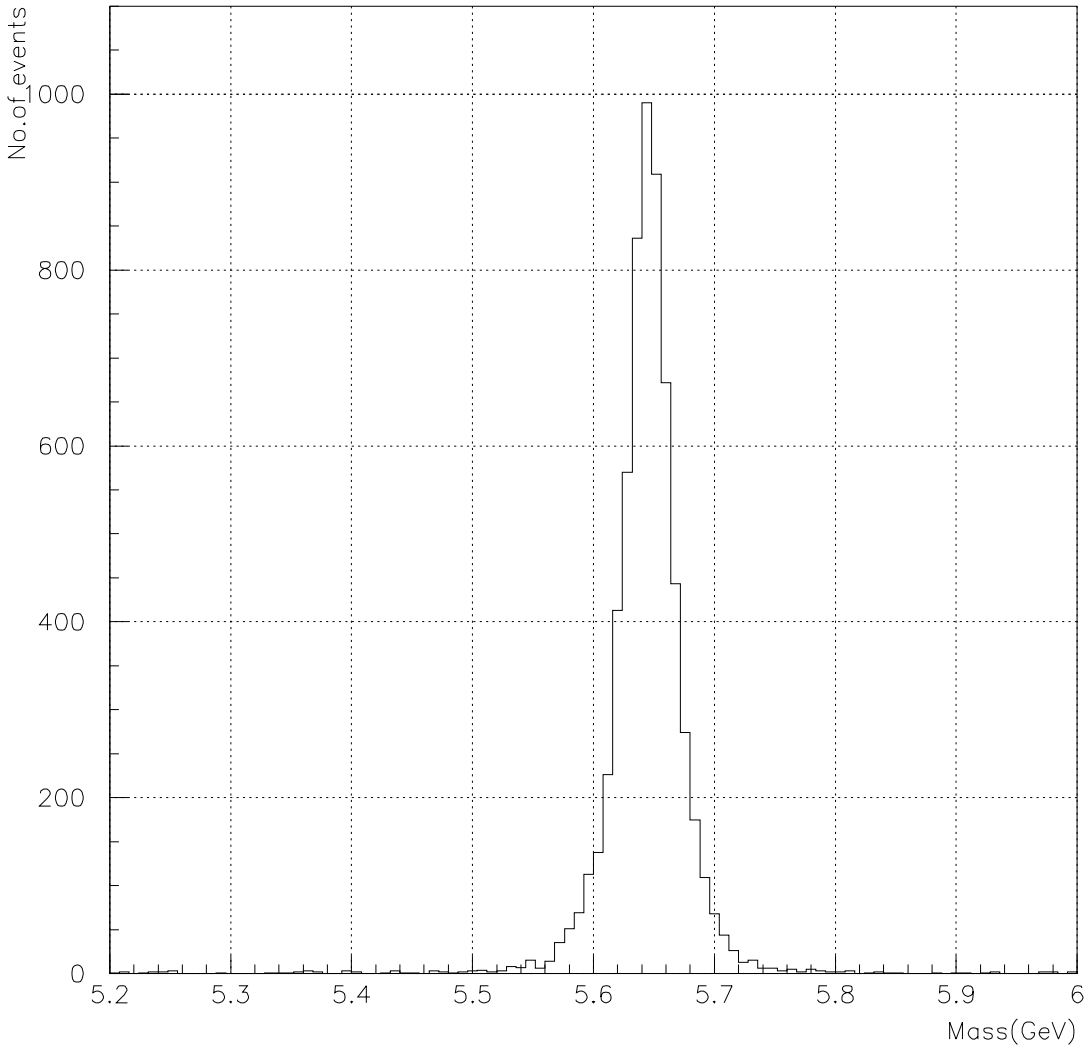

Figure 11: $J/\psi \oplus \Lambda_0$ invariant mass distribution after global fit

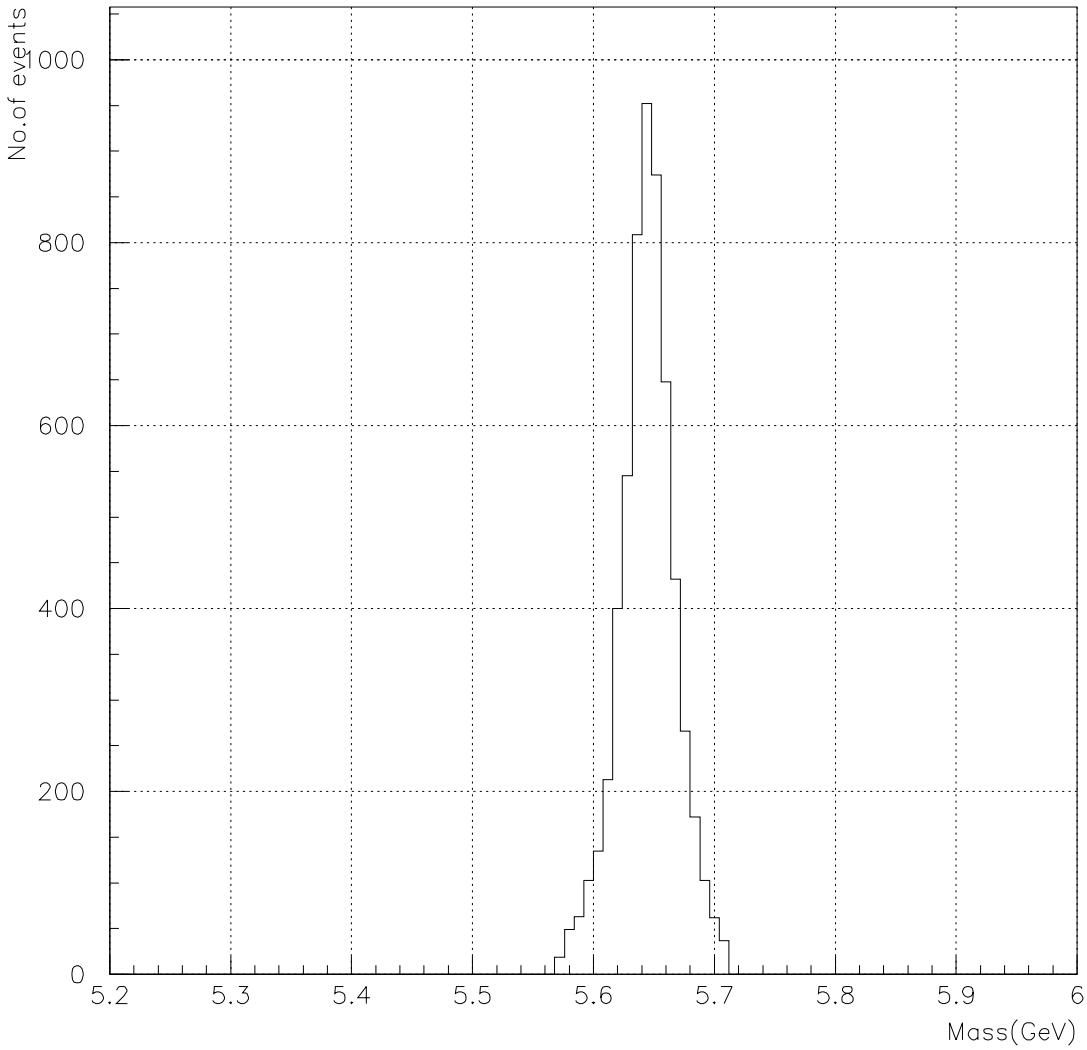

Figure 12: Fitted Λ_b invariant mass distribution. Gaussian fit to the peak gives $\sigma = 22MeV$. This histogram shows invariant mass of combinations $J/\psi \oplus \Lambda_0$ with positive global common vertex fit. Fitted Λ_b must have mass $\pm 70MeV$ around nominal Λ_b mass and proper time $\tau_{\Lambda_b} > 0.5ps$

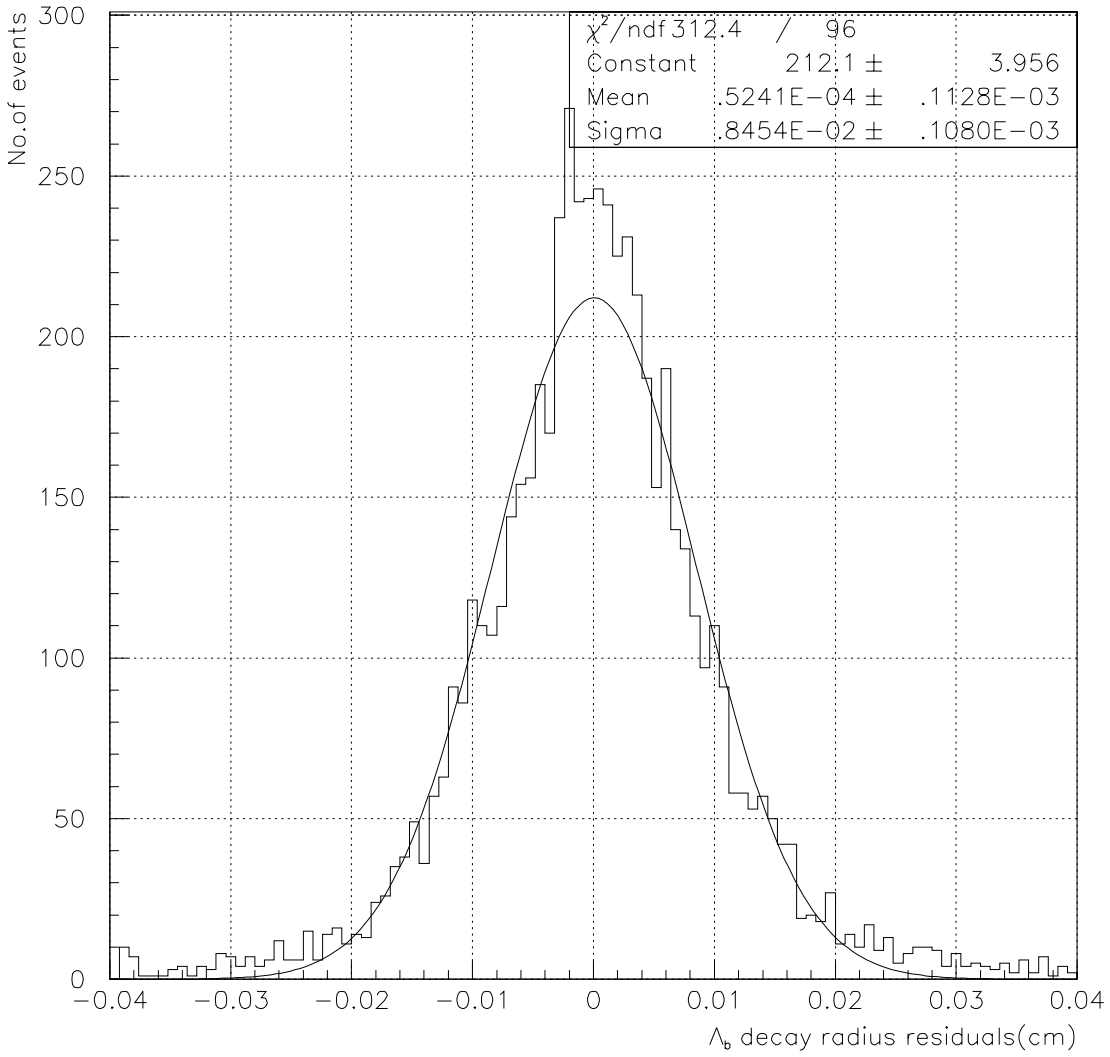

Figure 13: Λ_b decay radius residuals. Gaussian fit to the peak gives $\sigma = 84\mu m$

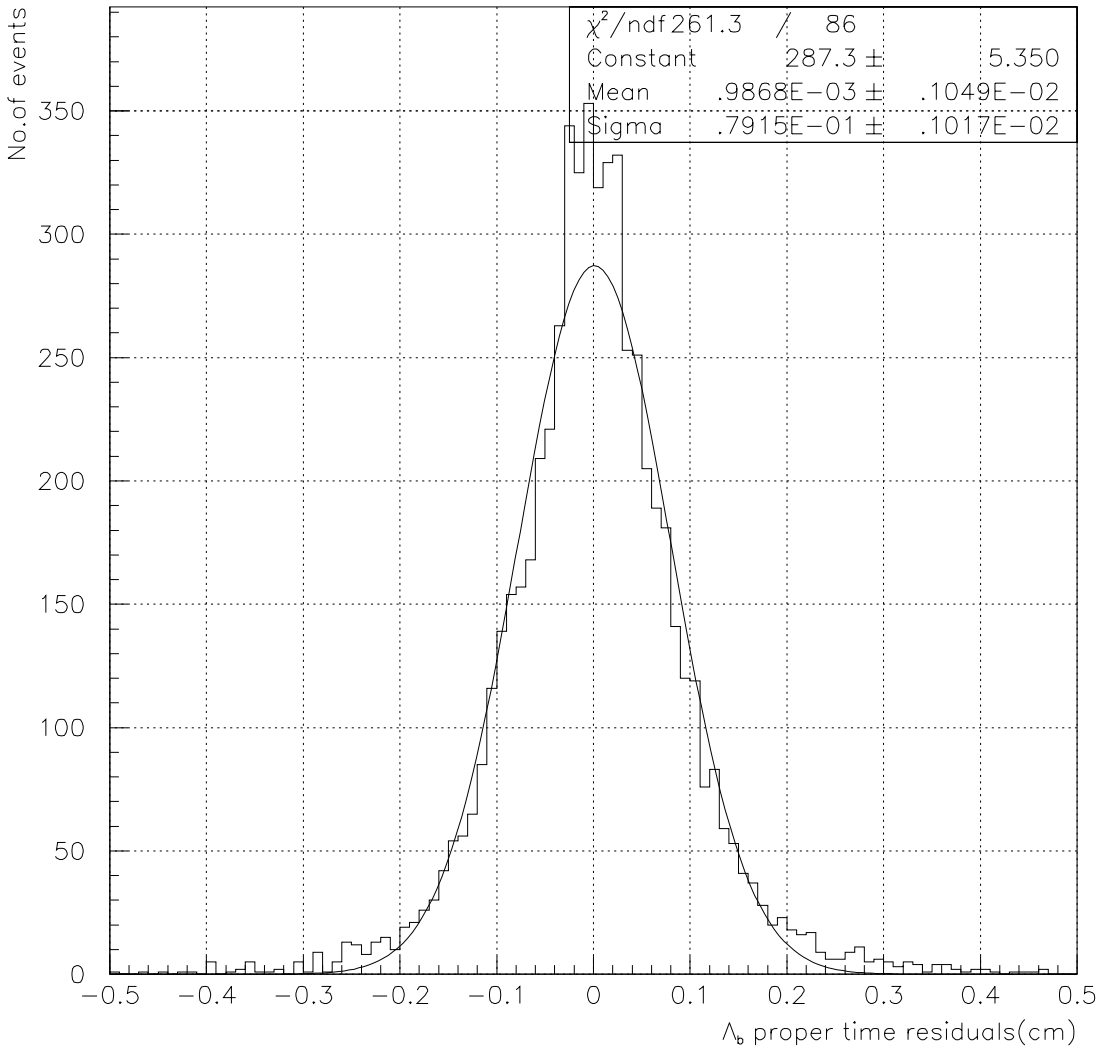

Figure 14: Λ_b proper time residuals. Gaussian fit to the peak gives $\sigma = 0.079ps$

6.3 Background-analysis results

Main background is dominated by real J/ψ and real Λ_0 produced in the primary interaction and fragmentation. The results of investigation of this background are summarized in Table 3. Next background processes are decay $\Xi_b^0 \to J/\psi\Xi_0(\to \Lambda_0\pi_0)$ and $\Xi_b^- \to J/\psi\Xi^-(\to \Lambda_0\pi^-)$. For first decay is background more important($\approx$ 20 percent). This background can be reduced by the minimal distance cut on between J/ψ and Λ_0(distance $d < 1.5mm$ gives dilution of 0.05). Background from $B_d \to J/\psi K_s$ where one pion is misidentified as proton is negligible after effective mass cuts. Background from fake J/ψ's can be effectivelly reduced using cut on minimal distance between primary vertex and the creation point of J/ψ. Background from

- $b \to J/\psi X$(inclusive J/ψ production)
- $b \to \mu(p_T > 6GeV)X$(inclusive μ production)

was estimated from results of fast ATLAS detector simulation(based on program ATLFAST and ATLFAST++)[16] made for process $B_d \to J/\psi K_s^0$. Summary information about above background processes are shown in Table 3. Number of signal events was taken from

parameter	**numerical value**
signal events	205500/year
reconstructed signal events	34524/year
$N(b \to J/\psi X)$	497/year
$N(b \to \mu(p_T > 6GeV)X)$	111/year
total background	608/year

Table 3: Summary information about background

$$N_s = L\sigma_{pyth}br(b \to \Lambda_b)br(\Lambda_b \to J/\psi\Lambda_0)br(J/\psi \to \mu\mu)$$

and these parameters are in Table 4. Cross section given by PYTHIA includes particle level cuts (i.e. signal events are $\Lambda_b \to J/\psi\Lambda_0$ events with $J/\psi \to \mu^+\mu^-$, $p_T^\mu > 6GeV$, $p_T^\mu > 3GeV$ in $|\eta| < 2.5$ and $\Lambda_0 \to p\pi$ with $p_T^{\pi,p} > 0.5GeV$ in $|\eta| < 2.5$)

parameter	**numerical value**
cross section given by PYTHIA	$\sigma_{pyth} = 0.183 \times 10^{-3}$mb
$br(b \to \Lambda_b)$	0.132
$br(\Lambda_b \to J/\psi\Lambda_0)$	0.014
$br(J/\psi \to \mu\mu)$	0.0602

Table 4: Value of cross section and branching ratios for process $\Lambda_b \to J/\psi\Lambda_0$

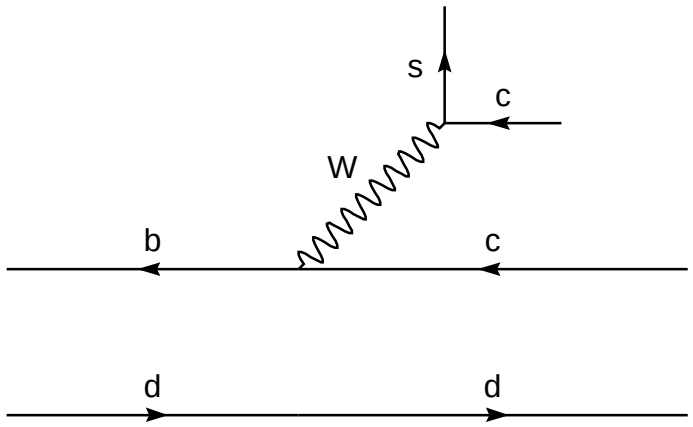

Figure 15: $B_d \to J/\psi K_0^*$ decay at quark level

7 CP violation in channel $B_d \to J/\psi K_0^*$

In this section I summarise my particle level results of analysis of channel $B_d \to J/\psi K_0^*$. At the quark level this process is caused by a weak charge current decay $b \to sc\bar{c}$(Fig.15) The process is an analog for decay $B_d \to J/\psi K_s$ and it's possible to extract CKM angle $\sin 2\beta$ from analysis therefore.

7.1 Theory

As has been said above higher orders weak interaction can cause transitions $B_0 \Leftrightarrow \bar{B}_0$ and therefore states B_0 and $\bar{B}_0$ aren't eigenstates of interaction hamiltonian. Owing to mixing B_0 meson can evolve to nontrivial combination $\alpha|B_0> + \beta|\bar{B}_0>$ and can be described by Schrödinger equation

$$i\frac{d}{dt}\begin{pmatrix}\alpha\\ \beta\end{pmatrix} = (M \Leftrightarrow \frac{i}{2}\Gamma)\begin{pmatrix}\alpha\\ \beta\end{pmatrix} \tag{40}$$

Here

$$(M \Leftrightarrow \frac{i}{2}\Gamma) = \begin{pmatrix} <B_0|H_W|B_0> & <B_0|H_W|\bar{B}_0> \\ <\bar{B}_0|H_W|B_0> & <\bar{B}_0|H_W|\bar{B}_0> \end{pmatrix} \tag{41}$$

and $M = M^\dagger$, $\Gamma = \Gamma^\dagger$ are 2×2 matrices. In case of CP conservation $M_{12} = M_{12}^*$ and $\Gamma_{12} = \Gamma_{12}^*$. CPT invariance guarantees that $M_{11} = M_{22}$ and $\Gamma_{11} = \Gamma_{22}$. Solutions of equation (40) are

$$|B^0_{phys}(t)> = e^{-i(m-i\frac{\Gamma}{2})t}(\cos\frac{\Delta M t}{2}|B^0> + i\frac{q}{p}\sin\frac{\Delta M t}{2}|\bar{B^0}>) \tag{42}$$

$$|\bar{B}^0_{phys}(t)> = e^{-i(m-i\frac{\Gamma}{2})t}(i\frac{p}{q}\sin\frac{\Delta M t}{2}|B^0> + \cos\frac{\Delta M t}{2}|\bar{B^0}> \tag{43}$$

where $p = \frac{1}{\sqrt{2}}(\alpha+\beta)$, $q = \frac{1}{\sqrt{2}}(\alpha \Leftrightarrow \beta)$, $m = \frac{M_{B_d}+M_{\bar{B}_d}}{2}$, $\Gamma = \frac{\Gamma_{B_d}+\Gamma_{\bar{B}_d}}{2}$ and $\Delta M = M_B \Leftrightarrow M_{\bar{B}}$. If the process conserves parity, we have $p = q$. Because the states $|B^0_{phys}>$ and $|\bar{B^0_{phys}}>$ are eigenstates of the H_W operator we can solve the usual eigenvalue problem

$$det(H_W \Leftrightarrow \lambda) = 0$$

and from this equation we can extract the ratio

$$\frac{q}{p} = \sqrt{\frac{M_{12}^* \Leftrightarrow \frac{i}{2}\Gamma_{12}^*}{M_{12} \Leftrightarrow \frac{i}{2}\Gamma_{12}}} \tag{44}$$

More precise theoretical calculation and experimental measurement show that $|M_{12}|$ is one half of mass difference between states $B_0, \bar{B_0}$ and analogically $|\Gamma_{12}|$ is one half of decay witdh difference between these states. For B-meson system is [30]

$$|M_{12}| \gg |\Gamma_{12}| \tag{45}$$

Using equation (1) we express ratio q/p in terms of CKM matrix elements

$$\frac{q}{p} = \frac{V_{tb}^* V_{td}}{V_{tb} V_{td}^*} = e^{-2i\beta} \tag{46}$$

7.2 Methods of CP violation measurement in $B_d \to J/\psi K_0^*$

There are two possibilities how to extract the value of $\sin 2\beta$. From the point of view of helicity formalism is the process $B_d \to J/\psi K_0^*$ described by three helicity amplitudes. In this decay helicity of J/ψ have to be the same as helicity of K^* because of B_0 zero spin. Let's assign these amplitudes as H_+, H_- and H_0.

$$H_+ =< B_d|T|J/\psi(+1)K_0^*(+1) > \tag{47}$$

$$H_- =< B_d|T|J/\psi(\Leftrightarrow 1)K_0^*(\Leftrightarrow 1) > \tag{48}$$

$$H_0 =< B_d|T|J/\psi(0)K_0^*(0) > \tag{49}$$

where ± 1 and 0 stand for helicity. If we describe any process with help of state vector $|\vec{p} = 0, \lambda >$(CMS frame) then for CP conjugated state vector holds $CP|\vec{p} = 0, \lambda > \approx |\vec{p} = 0, \Leftrightarrow \lambda >$. It's clear that only states with zero helicity are eigenstates of CP operator. This is the case of $B_d \to J/\psi K_s$ decay. So if we extract the ratio of decay to states with zero helicity we can work in total analogy with the decay $B_d \to J/\psi K_s$ i.e. measure the asymmetry(see sect.4.1)

$$a_{CP} = \frac{\Gamma(B_d \to J/\psi(0)K_0^*(0)) \Leftrightarrow \Gamma(\bar{B_d} \to J/\psi(0)K_0^*(0))}{\Gamma(B_d \to J/\psi(0)K_0^*(0)) + \Gamma(\bar{B_d} \to J/\psi(0)K_0^*(0))} \tag{50}$$

Such an extraction can be performed with help of angular analysis of cascade decay $B_d \to J/\psi K_0^*(\to K_0\pi_0)$. For this angular distribution we can write down [29]

$$\frac{d\Gamma}{d\Omega} = \sum_{\lambda=\pm1,0} \Gamma(B_d \to J/\psi(\lambda)K^*(\lambda)) \frac{d\Gamma(K^*(\lambda) \to K_0\pi_0)}{d\Omega} \tag{51}$$

Using helicity formalism we see that

$$\frac{d\Gamma(K^* \to K_0\pi_0)}{d\Omega} = \sum_{MN} \mathcal{D}^{1*}_{M0}(\phi\theta \Leftrightarrow \phi)\mathcal{D}^{1}_{N0}(\phi\theta \Leftrightarrow \phi) \tag{52}$$

and after explicit calculation we get

$$\frac{d\Gamma(B_d \to J/\psi K^*(\to K_0\pi_0))}{d\Omega} = a + b\sin^2\theta \tag{53}$$

where θ is the angle between K_0 momentum and K^* momentum in K^* rest frame,

$$a \approx \Gamma(B_d \to J/\psi(0)K^*(0))$$

and b is a function of all helicity widths. Thus the θ-independent part of this distribution is the zero-helicity fraction. The experimental value of the zero-helicity fraction 0.8 ± 0.08[24] shows, that this amplitude dominates the decay.

More precise results can be achieved by using full angular information. This method first proposed in [25] use full angular distribution of above cascade decay. This method is based on helicity amplitudes parametrization by strong and weak phases. Owing to B meson mixing here are two contributions with different weak phases. The difference of these phases is equal to 2β. Total angular distribution of cascade decay $B_d \to J/\psi(\to e^-e^+)K^*(\to K_0\pi_0)$ can be written as

$$W(\theta_1, \theta_2, \phi) = \frac{9p}{16m^2\pi^2} \sum_{i=1}^{i=8} G_i(\theta_1, \theta_2, \phi)X_i \tag{54}$$

In this distribution θ_1 is the polar angle of K_0 momentum in K^* rest frame , θ_2 and ϕ are polar and azimuthal angles of positron momenta in J/ψ rest frame, $p = |\vec{p}_{J/\psi}| = |\vec{p}_{K^*}|$ and m is B_d mass [15].

i	G_i	X_i
1	1	1
2	$d^2_{00}(\theta_1)$	$\Leftrightarrow H_+H_+^* \Leftrightarrow H_-H_-^* + 2H_0H_0^*$
3	$d^2_{00}(\theta_1)$	$\frac{1}{2}H_+H_+^* + \frac{1}{2}H_-H_-^* \Leftrightarrow H_0H_0^*$
4	$d^2_{00}(\theta_1)d^2_{00}(\theta_2)$	$\Leftrightarrow\frac{1}{2}H_+H_+^* \Leftrightarrow\frac{1}{2}H_-H_-^* + 2H_0H_0^*$
5	$\cos 2\phi d^2_{20}(\theta_1)d^2_{20}(\theta_2)$	$\Leftrightarrow 6Re(H_+H_-^*)$
6	$\sin 2\phi d^2_{20}(\theta_1)d^2_{20}(\theta_2)$	$6Im(H_+H_-^*)$
7	$\cos \phi d^2_{10}(\theta_1)d^2_{10}(\theta_2)$	$\Leftrightarrow 3Re(H_+H_0^* + H_-H_0^*)$
8	$\sin \phi d^2_{10}(\theta_1)d^2_{10}(\theta_2)$	$3Im(H_+H_0^* \Leftrightarrow H_-H_0^*)$

Table 5: X_i and G_i functions appearing in B_d decay angular distribution (54). Here $d^2_{00}(\theta) = \frac{1}{2}(3\cos^2\theta - 1)$, $d^2_{10}(\theta) = -\sqrt{\frac{3}{2}}\sin\theta\cos\theta$ and $d^2_{20}(\theta) = \frac{\sqrt{6}}{4}\sin^2\theta$ are rotation function[27]

Functions G and X are listed in Table 5. This angular distribution is valid for B_d decay. For $\bar{B}_d$ decay an analogical shape of angular distribution holds. We see that(Table 6)

$$\bar{W}(\theta_1, \theta_2, \phi) = \frac{9p}{16m^2\pi^2}\sum_{i=1}^{i=8} G_i(\theta_1, \theta_2, \phi)\bar{X}_i \tag{55}$$

Momets X_i(7 moments) can be written also in terms of definite CP

i	G_i	X_i
1	1	1
2	$d^2_{00}(\theta_1)$	$\Leftrightarrow\bar{H}_+\bar{H}_+^* \Leftrightarrow\bar{H}_-\bar{H}_-^* + 2\bar{H}_0\bar{H}_0^*$
3	$d^2_{00}(\theta_1)$	$\frac{1}{2}\bar{H}_+\bar{H}_+^* + \frac{1}{2}\bar{H}_-\bar{H}_-^* \Leftrightarrow\bar{H}_0\bar{H}_0^*$
4	$d^2_{00}(\theta_1)d^2_{00}(\theta_2)$	$\Leftrightarrow\frac{1}{2}\bar{H}_+\bar{H}_+^* \Leftrightarrow\frac{1}{2}\bar{H}_-\bar{H}_-^* + 2\bar{H}_0\bar{H}_0^*$
5	$\cos 2\phi d^2_{20}(\theta_1)d^2_{20}(\theta_2)$	$\Leftrightarrow 6Re(\bar{H}_+\bar{H}_-^*)$
6	$\sin 2\phi d^2_{20}(\theta_1)d^2_{20}(\theta_2)$	$6Im(\bar{H}_+\bar{H}_-^*)$
7	$\cos \phi d^2_{10}(\theta_1)d^2_{10}(\theta_2)$	$\Leftrightarrow 3Re(\bar{H}_+\bar{H}_0^* + \bar{H}_-\bar{H}_0^*)$
8	$\sin \phi d^2_{10}(\theta_1)d^2_{10}(\theta_2)$	$3Im(\bar{H}_+\bar{H}_0^* \Leftrightarrow\bar{H}_-\bar{H}_0^*)$

Table 6: $\bar{X}_i$ and G_i functions appearing in $\bar{B}_d$ decay angular distribution (60)

quantities

$$Q_+ \equiv H_+ + H_- \tag{56}$$

$$Q_- \equiv H_+ \Leftrightarrow H_- \tag{57}$$

$$Q_0 \equiv H_0 \tag{58}$$

New moments Q_+, Q_0 have negative CP parity and Q_- positive. Depending on relative strenghts of different CP contributions, the moments X_i will show different CP asymmetries. Linear combinations of X_i can give undiluted asymmetry measurements by extracting quantities

$$Q_+Q_+^*, \quad Q_-Q_-^*, \quad Q_0Q_0^*, \quad ReQ_+Q_0^* \tag{59}$$

or their $\bar{B}$ counter parts

$$\bar{Q}_+\bar{Q}_+^*, \quad \bar{Q}_-\bar{Q}_-^*, \quad \bar{Q}_0\bar{Q}_0^*, \quad Re\bar{Q}_+\bar{Q}_0^* \tag{60}$$

Helicity amplitudes(H or Q) have 5 independent parameters:two modules, two relative phases from strong interaction and weak phase difference which is equal to 2β(the angle is defined by CKM matrix and is the same as for $B_d \to J/\psi K_s^0$).
Weak phase can be extracted from CP-definite quantities as for example

$$\frac{Q_+Q_+^* \Leftrightarrow \bar{Q}_+\bar{Q}_+^*}{Q_+Q_+^* + \bar{Q}_+\bar{Q}_+^*} = \sin 2\beta \frac{x_d}{1+x_d^2} \tag{61}$$

where $x_d = \frac{\Delta M_B}{\Gamma_B} \approx 0.73$ is B_d mixing parameter(see chapter 4.3). The other 4 parameters can be derived also from untaged samples $B_d \to J/\psi K^*(\to K_0\pi_0)$ or from isospin related samples $B_d \to J/\psi K^*(\to K_+\pi_-)$ to increase the statistical precision.
The parameters can be extracted either by maximum likelyhood fit, or by method of moments. The later method is based on the fact that angular coefficients $G_i(\theta_1, \theta_2, \phi)$ are experimental observables. We will measure their expectation values

$$< G_i(\theta_1, \theta_2, \phi) >= \frac{1}{N_s} \sum_{k=1}^{k=N_s} G_i^k(\theta_1, \theta_2, \phi) \tag{62}$$

where N_s is number of measured events. On the other side we have

$$< G_i(\theta_1, \theta_2, \phi) >= \frac{\int\int\int W(\theta_1, \theta_2, \phi) G_i(\theta_1, \theta_2, \phi) d\cos\theta_1 d\cos\theta_2 d\phi}{\int\int\int W(\theta_1, \theta_2, \phi) d\cos\theta_1 d\cos\theta_2 d\phi} \tag{63}$$

where $W(\theta_1, \theta_2, \phi)$ may be (54) or (55), or their difference or their sum in the case of tagged samples. is the difference of B and $\bar{B}$ angular distributions. Equations (63)(the one for each i) leads to a system of seven equation for seven helicity coefficients $X_i(\bar{X}_i)$. If we solve these equation we can express coefficients $X_i(\bar{X}_i)$ in terms of expectation values $< G_i(\theta_1, \theta_2, \phi) >$.

7.3 Particle level study of $B_d \to J/\psi K_0^*$

Number of such events produced per year at initial low luminosity($L = 10^{33} cm^{-2} s^{-1}$) is

$$N_s = L\sigma_{pyth} br(b\bar{b} \to B_d \mu X) br(B_d \to J/\psi K^*) br(J/\psi \to e^+e^-) \sim 3200 \tag{64}$$

where $\sigma_{pyth} = 0.31 \times 10^{-4} mb$ is cross section given by PYTHIA(this includes selection cuts given below). I restrict myself to particle level results of simulations of this channel. For this purpose about 2000 signal events of type $b\bar{b} \to \mu BX \to B(J/\psi K^*)$ has been generated by B-Atgen based on PYTHIA. Event was accepted if (particle level conditions)

1. $J/\psi \to e^+e^-$ and electrons have $p_T > 0.5 GeV$ in $|\eta| < 2.5$
2. $K^* \to K_0(\to \pi^+\pi^-)\pi_0(\to \gamma\gamma)$, charged pions must have $p_T > 0.5 GeV$ in $|\eta| < 2.5$ and energy of each γ, $E_\gamma > 1 GeV$ in $|\eta| < 2.5$
3. there must be a LVL1 trigger muon coming from semileptonic decay of second b-quark

I analyzed events with such properties by GENZ package. In a real experiment J/ψ will be reconstructed in the inner detector as well

as K_s coming from K^* decay. Neutral pion will be reconstructed in the electromagnetic calorimeter. π_0 reconstruction causes large problem as we will see later. I studied three types of background taken from signal events($bB_d \to J/\psi K^* \mu X(K^* \to K_0\pi_0)$) and from events $b\bar{b} \to J/\psi\mu X$.

- real $J/\psi\oplus$ real K_s
- real $J/\psi\oplus$ real $K_s\oplus$ real π_0
- real $J/\psi\oplus$ real $K_s\oplus$ real $\gamma\oplus$ real γ)

Here $\oplus$ means that particles are not necessary coming from the same decay and combined particles must satisfy particle level conditions 1,2.

7.3.1 real $J/\psi\oplus$ real K_s combinations

Here all J/ψ and K_s has been combined. Particles in combinations must satisfy particle level conditions(1,2) and in addition K_s decay radius must be in $< 1,44 > cm$(see Fig.20). This requirement is the only one that reduces signal. Corresponding reduction factor is ~ 0.74. These combination are the auxiliary ones. They are performed because the strongest backgroung to signal decay is the decay $B_d \to J/\psi K_s$. Next useful cut is that we require the angle between momentum of composed $J/\psi \oplus K_s$ and B_d meson momentum to be less than 0.18 radians. Distribution of this angle is shown in Fig.19. We suppose that K_s comes from strong decay of K^*. Such process is very quick($\sim 10^{-23}s$) and therefore we require the distance of closest approach of J/ψ momentum vector and K_s creation point to be less than $100\mu m$.Finally invariant mass distribution for signal combinations is shown in Fig.16. From this picture it is clear that's useful to require $M_{J/\psi\oplus K_s} < 5.2GeV$. All cuts used for $J/\psi\oplus K_s$ combinatorial background reduction are

1. mass $M_{J/\psi\oplus K_s} < 5.2GeV$
2. distance of closest approach of J/ψ momentum vector and K_s creation point to be less than $100\mu m$

3. angle between momentum vector of composed $J/\psi \oplus K_s$ and B_d meson momentum vector to be less than 0.18 radians

4. K_s decay radius $1 < R_K < 44$ cm

7.3.2 real $J/\psi\oplus$ real $K_s\oplus$ real π_0 combinations

This is an analog of later combination. The cuts are

1. invariant mass of $J/\psi \oplus K_s, M_{J/\psi\oplus K_s} < 5.2GeV$

2. distance of closest approach of J/ψ momentum vector and K_s creation point to be less than $100\mu m$

3. angle between momentum of composed $J/\psi \oplus K_s$ and B_d meson momentum to be less than 0.18 radians

4. K_s decay radius $1 < R_K < 44$ cm

5. enegry of neutal pion must be greater than 2 GeV

6. invariant mass of $K_s \oplus \pi_0, M_{K_s\oplus\pi_0} \in < \Leftrightarrow 150, 150 > MeV$ around nominal K_0^* mass

7. invariant mass of $J/\psi \oplus K_s \oplus \pi_0, M_{J/\psi\oplus K_s\oplus\pi_0} \in < \Leftrightarrow 300, 300 > MeV$ around nominal B_0 mass

7.3.3 real $J/\psi\oplus$ real $K_s \oplus \gamma \oplus \gamma$ combinations

These combinations will be important for experimental B_d reconstruction. Two gammas will be reconstructed in the electromagnetic calorimeter. Applied cuts are

1. invariant mass of $J/\psi \oplus K_s, M_{J/\psi\oplus K_s} < 5.2GeV$

2. distance of closest approach of J/ψ momentum vector and K_s creation point to be less than $100\mu m$

3. angle between momentum of composed $J/\psi \oplus K_s$ and B_d meson momentum to be less than 0.18 radians

4. K_s decay radius $1 < R_K < 44$ cm

5. energies of both gammas must be greater than $1GeV$

6. angle between gammas momenta(in 3D) must be less than 0.18 radians

7. invariant mass of gammas $M_{\gamma\oplus\gamma} \in < \Leftrightarrow 60, 60 > MeV$ around nominal π_0 mass

8. invariant mass of $K_s \oplus \gamma \oplus \gamma$,$M_{K_s\oplus\gamma\oplus\gamma} \in < \Leftrightarrow 150, 150 > MeV$ around nominal K_0^* mass

9. invariant mass of $J/\psi\oplus K_s\oplus\gamma\oplus\gamma$, $M_{J/\psi\oplus K_s\oplus\gamma\oplus\gamma} \in < \Leftrightarrow 300, 300 > MeV$ around nominal B_d mass

Summary information about above three types of combinatorial background for events $bB_d \to J/\psi K^*(K_0\pi_0)\mu X$ and $b\bar{b} \to J/\psi\mu X$ are in Table 9.

7.4 π_0 reconstruction in electromagnetic calorimeter

As has been said π_0 will be reconstructed in the electromagnetic calorimeter. Main principle of reconstruction is the identification of two electromagnetic clusters created by photons coming from $\pi_0 \to \gamma\gamma$ decay. For good π_0 mass reconstruction and identification photons must have energies greater than $1GeV$(i.e.π_0 energy must be greater than $2GeV$)[26]. Next very strong condition is that space angle between two photons must be greater than 0.1 radians[26]. From kinematics we can easily find the relation

$$E_{\pi_0} = \frac{m_\pi}{\sin\frac{\theta}{2}} \tag{65}$$

where m_π is pion mass, E_γ is photon energy(I suppose that $E_\gamma^1 \approx E_\gamma^2$) and θ is angle between photons. This dependence is shown in Fig.17 for signal photons. We can see that fraction of events with these conditions($E_{\pi_0} > 2GeV$ and $\prec(\gamma\gamma) > 0.1$ radians) is less than 5%. Therefore these conditions strongly reduce signal. This large

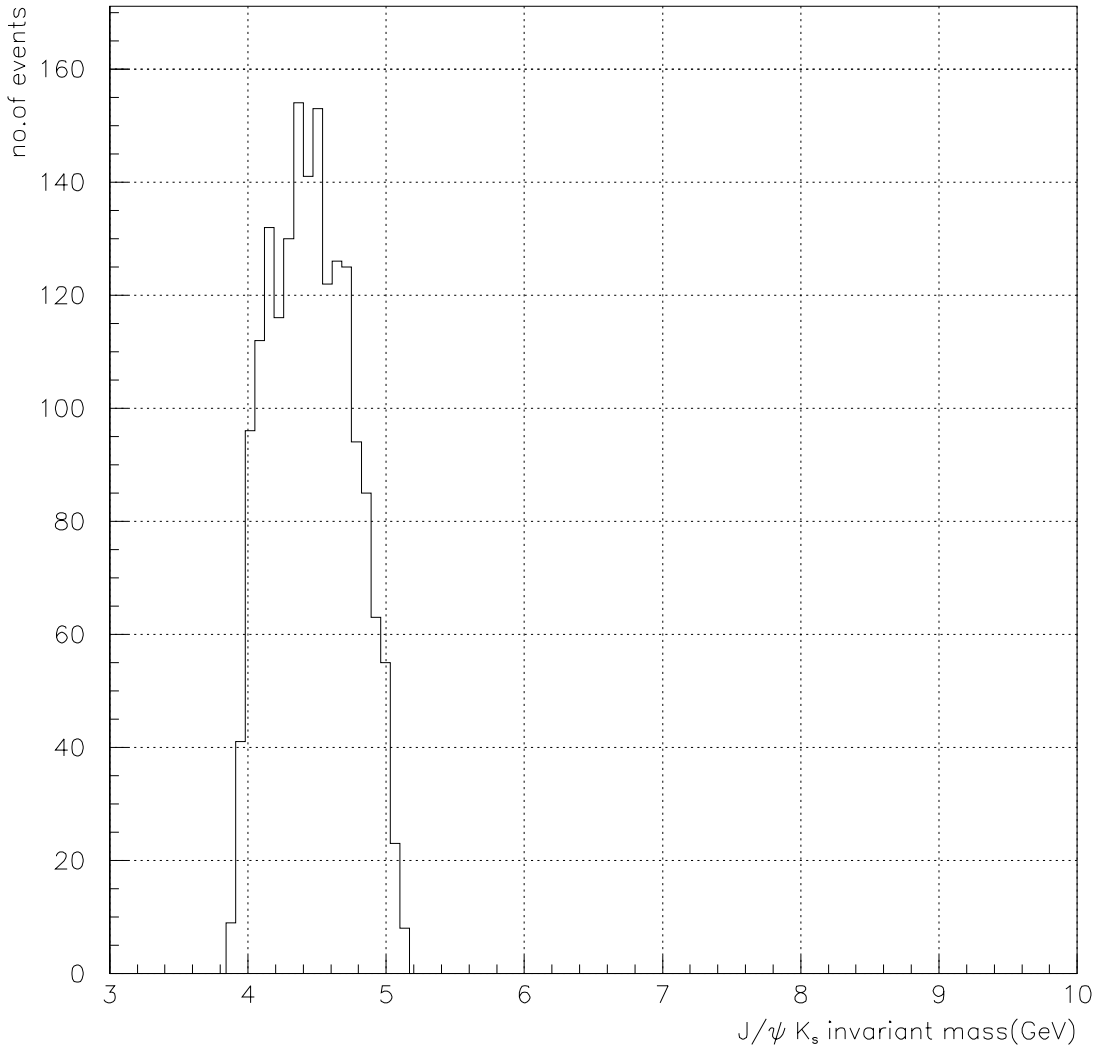

Figure 16: Signal $J/\psi K_s$ invariant mass distribution

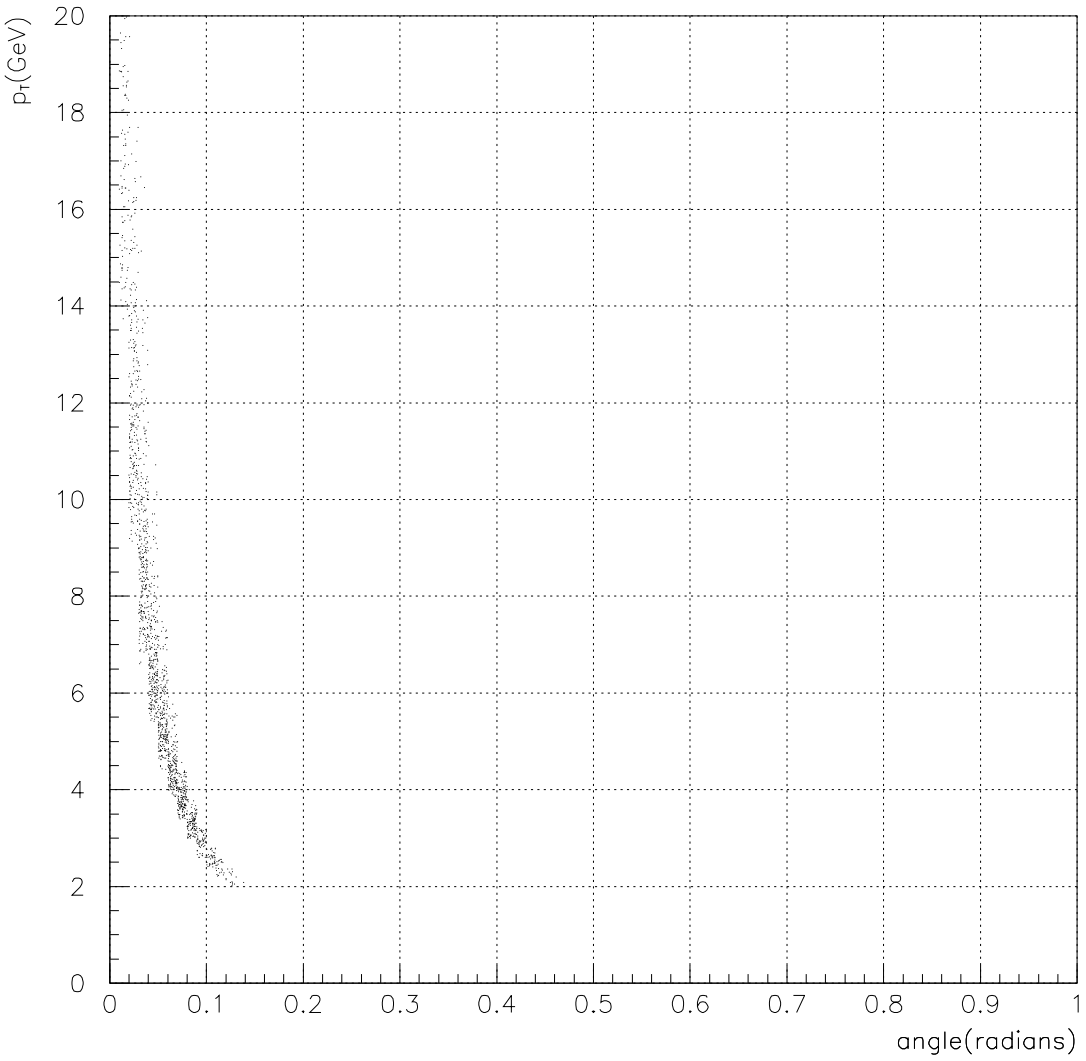

Figure 17: Energy of signal π_0 as a function of $\gamma\gamma$ angle for signal events

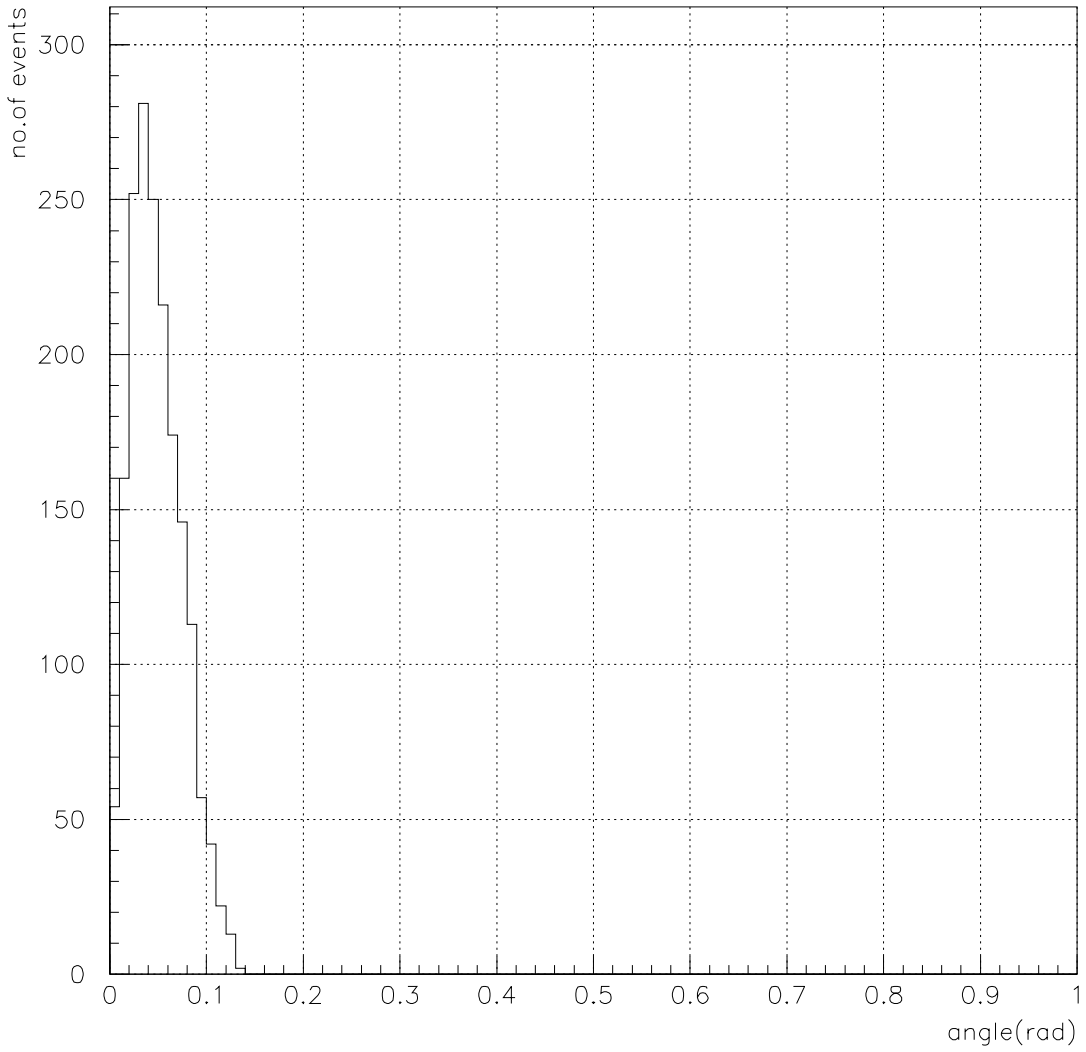

Figure 18: Distribution of space angle between photons from signal π_0 decay

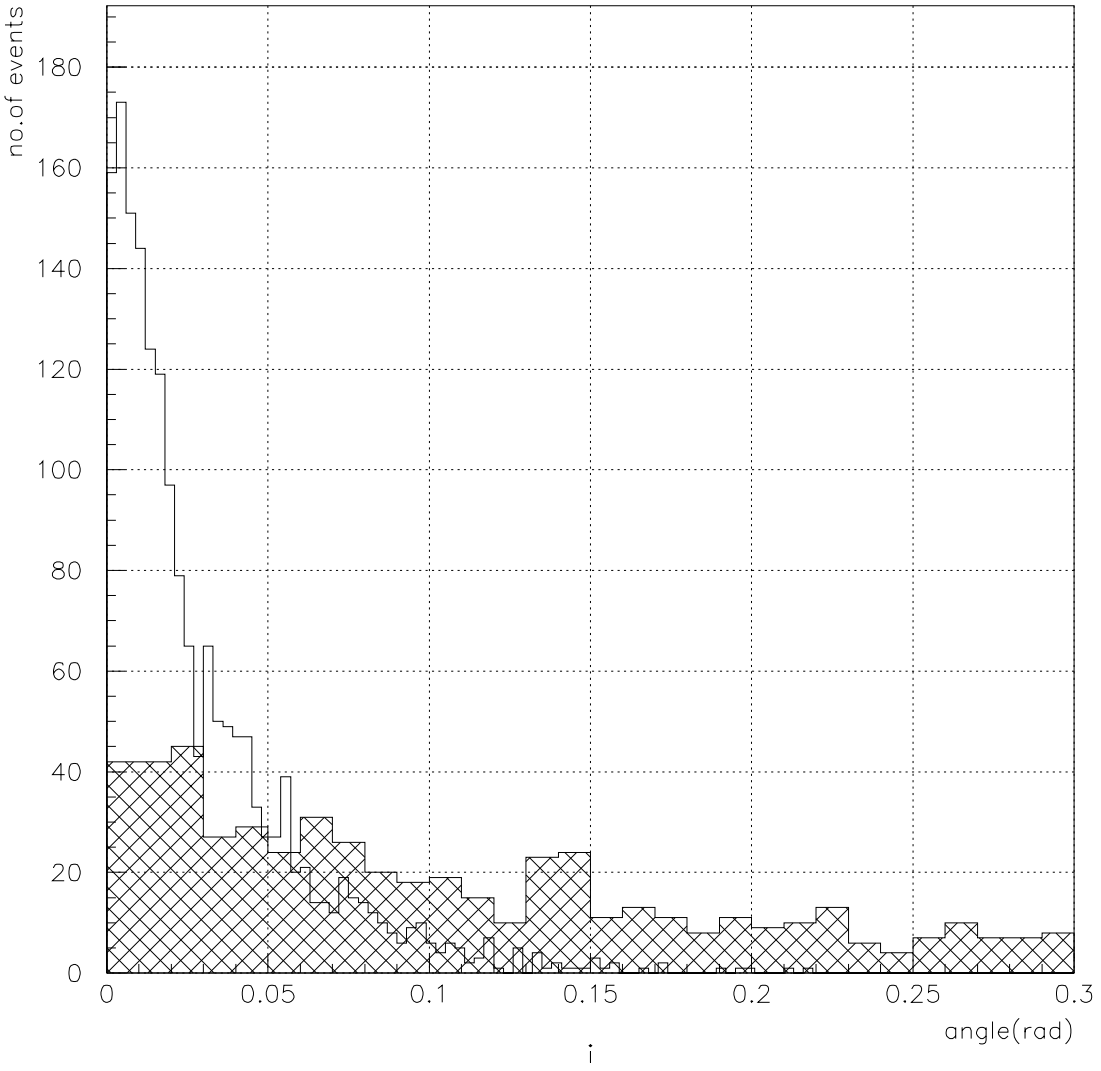

Figure 19: Distribution of angle between $J/\psi K_s$ momentum and B_d momentum for signal(white) and combinatorial background(dashed)

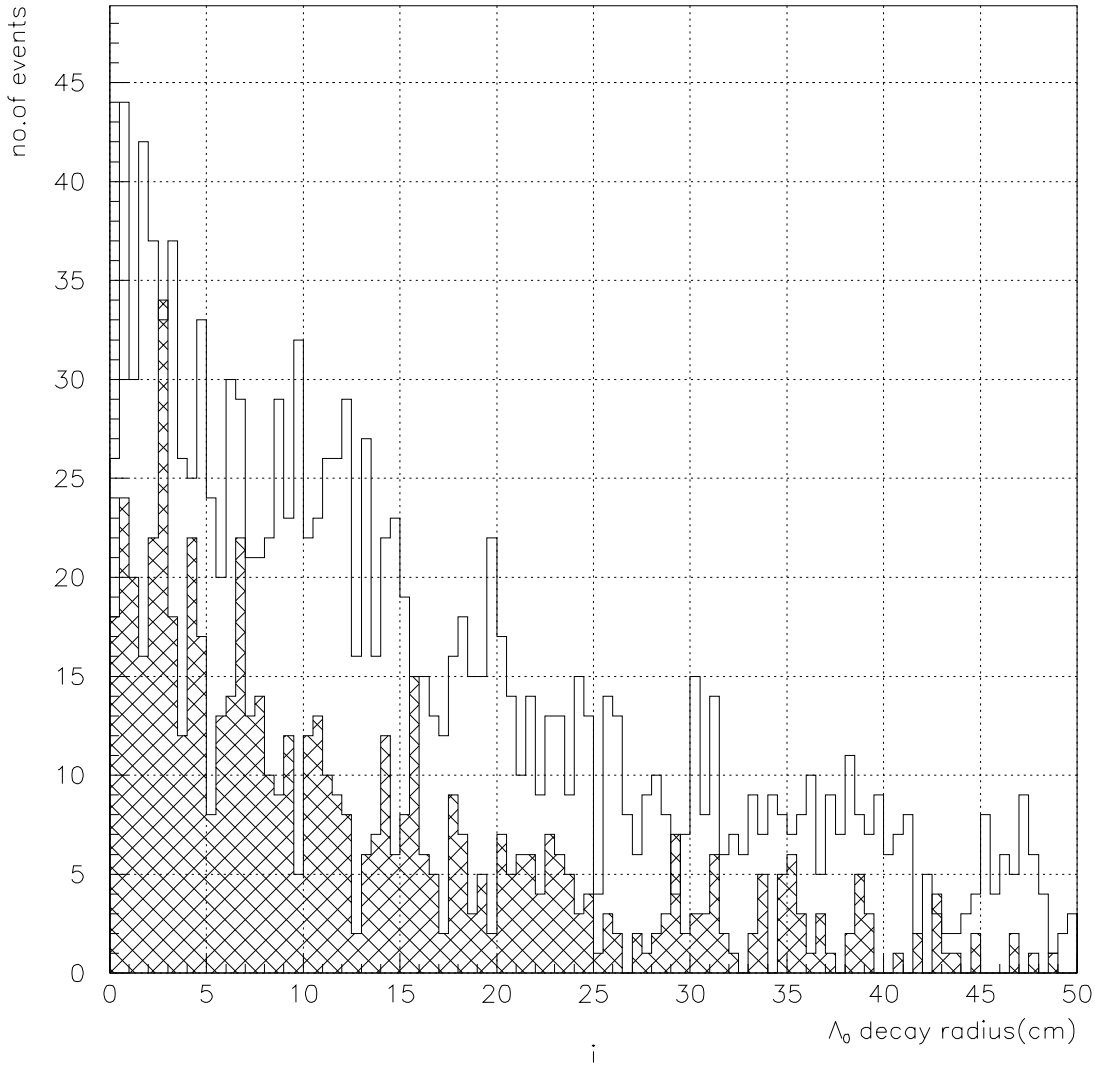

Figure 20: Distribution of decay radius of K_s for signal(white) and combinatorial background(dashed)

reduction is important for determination of signal/background ratio and for discussion about feasibility of measurement of $\sin 2\beta$ in decay $B_b \to J/\psi K_0^*$(see section 7.6).

7.5 Background-analysis results

Main background to signal chain $B_d \to J/\psi K_0^*$ comes from inclusive J/ψ production processes(i.e.from processes $b \to J/\psi X$). The strongest process of this type is $B_d \to J/\psi K_s$. Using the cuts presented in sect.7.3. I reduced background from processs $B_d \to J/\psi K_0$ to negligible level(see Table 9.in Appendix). For ratio signal/background holds relation

$$R = \frac{br(B_d \mu X) br(J/\psi K^*) br(K_0 \pi_0) br(K_s) br(\gamma\gamma)}{br(J/\psi \mu X)} \tag{66}$$

where branching ratios are listed in next Table 7.

branching	**numerical value**
$br(B_d \mu X) = br(b\bar{b} \to B_d \mu X)$	0.04
$br(J/\psi K^*) = br(B_d \to J/\psi K^*)$	0.0016
$br(K_0 \pi_0) = br(K^* \to K_0 \pi_0)$	0.33
$br(K_s) = br(K_0 \to K_s)$	0.5
$br(\gamma\gamma) = br(\pi_0 \to \gamma\gamma)$	0.99
$br(J/\psi \mu X) = br(b\bar{b} \to J/\psi \mu X)$	0.0012

Table 7: Branching ratios of subprocesses

Using explicit values of above branchings we could get the result $R = 5.89 \times 10^{-3}$. For total ratio signal/background we must write down relation

$$R_{tot} = R \frac{\Delta_\pi^{sig}}{\Delta_\pi^{bck}} \frac{\Delta^{K_s}}{\Delta_{bck}^{tot}} \Delta(\pi\gamma) \tag{67}$$

where

- Δ_π^{sig} and Δ_π^{bck} are efficiencies of π_0 reconstruction in electromagnetic calorimeter for signal pions and for pions coming from background(I suppose that $\Delta_\pi^{sig} \sim \Delta_\pi^{bck}$).

- $\Delta^{K_s} = 0.74$ is reduction factor coming from requirement of decay radius of K_s within $< 1, 50 > cm$.
- $\Delta^{tot}_{bck} = 1.98 \times 10^{-4}$ is background reduction factor
- $\Delta(\pi\gamma) = 0.045$ is reduction factor coming from precise π_0 reconstruction in electromagnetic calorimeter(i.e.$E(\pi_0) > 2GeV$ and $\prec (\gamma\gamma) > 0.1$rad).

With these values

$$R_{tot} < 0.99 \tag{68}$$

and therefore main result is that background $\sim$ signal. This is the upper limit on R_{tot} because the special process $B_d \to J/\psi K_s$ has been studied in place of the general process $b \to J/\psi X$

7.6 CP violation in $B_d \to J/\psi K^*_0$-feasibility of measurement

The equation (67) for signal/background ratio can be rewritten as

$$R_{tot} < 22.05\Delta(\pi\gamma)$$

(i.e.background form about 4% if $\Delta(\pi\gamma) = 1$). From this shape is apparent that main problem is caused by π_0 reconstruction requirements. Neutral pions will be reconstructed in the electromagnetic calorimeter. Both photons coming from $\pi_0 \to \gamma\gamma$ are identified as electromagnetic clusters. These clusters are assigned as photons and their invariant mass is a mass of reconstructed pion. Requirements $E_\gamma > 1GeV$ and angle between gammas greater than 0.1 radians can be abandoned but in this case all electromagnetic cluster algorithms fail because of large smearing of invariant mass of reconstructed pion. Global result is therefore that this channel cannot be used (at present electromagnetic calorimeter evolution) for $\sin 2\beta$ measurement due to lack of statistics. If we have about 3200 signal events per year then after π_0 reconstruction we get

$$N_{rec} = N_s\Delta(\pi\gamma) \approx 144$$

events per year. From equation(10) we see that statistical error of $\sin 2\beta$ depends on number of reconstructed events

$$\delta(\sin 2\beta) \approx \frac{1}{\sqrt{N_{rec}}}$$

Using equation(10) and values of $\sqrt{D_{tag}}$=0.7 and D_{tag}=0.56, D_{int}=0.62 (taken from [16]) we get

$$\delta(\sin 2\beta) < 0.25$$

and it's apparent that measurement of $\sin 2\beta$ is meaningless at this statistical level. Larger statistics contribution will come from channel $B_d \to J/\psi K_0^*$ because in this case tags using the jet charge and charge of associated pions can be involved and trigger can be obtain from one of J/ψ muons.

8 Conclusions

As it's shown in chapter 6 we expect number of reconstructed $\Lambda_b \to J/\psi\Lambda_0$ events to be about 34530 per year. Using the helicity method and least square method we can calculate the maximal statistical error on polarization. This error is 0.025. In this thesis I studied muonic channel only($J/\psi \to \mu^+\mu^-$). An analogical reconstruction can be performed for electron channel($J/\psi \to e^+e^-$) which increase statistics of reconstructed events and therefore also the error on polarization will be less than 0.025.
The strongest background coming from inclusive J/ψ production($b \to J/\psi X$) and inclusive muon production($b \to \mu(p_T > 6)X$) can be reduced to $\sim$ 1.7%. In this thesis I show that process $\Lambda_b \to J/\psi\Lambda_0$ is the good sample for polarization measurements.

Next process studied was $B_d \to J/\psi K^{0*}$. Fesibility study on CP violation measurement in this process has been performed in one channel($J/\psi \to e^+e^-$) and this study was based on the PYTHIA program results. The precision of $\sin 2\beta$ measurement suffers mainly

due to strong statistics reduction in neutral pion reconstruction in the electromagnetic calorimeter(reduction factor $\sim$0.045).
Also background events has been studied. The most significant background are inclusive J/ψ production events. In place of the general process($b \to J/\psi X$) a special process $B_d \to J/\psi K_s$ of this type has been studied and results from this analysis was applied for process $b \to J/\psi X$. Therefore I found upper limits on ratio of signal/background and on the error on $\sin 2\beta$ only.

References

[1] M.Smizanska et al., J.Phys. G:Nucl. Part. Phys. 21(1995) 629-638

[2] R.Lednicky, Yad.Fiz.43, 1275-1281(May 1986)

[3] R.Lednicky, DrSc Thesis, JINR-Dubna 1990

[4] A.Ballestrero, E.Maina: A new method of helicity calculations, hep-ph 9403244

[5] M.Jacob, J.C.Wick, Ann.Phys.7(1959) 404

[6] I.I.Bigi, CERN-TH 7207/94

[7] P.Eerola et al., ATLAS Internal Note PHYS-NO-054 15 December 1994

[8] G.C.Branco, CERN-TH 7176 February 1994

[9] A.Kotanski, K.Zalewski, Nucl.Phys.B4(1968) 559-572

[10] J.D.Richman, PhD thesis, CALT-68-1148

[11] M.Anselmino et al., Helicity formalism and spin effects, CB PF-NF-045/90

[12] M.Krämer et al., Z.Phys.C57, 115-134(1993)

[13] I.Dunietz, SLAC-PUB-5270, November 1990

[14] G.Kramer, B.Palmer, preprint DESY 91-134 November 1991

[15] G.Kramer et al., preprint DESY 93-192 December 1993

[16] G.F.Tartarelli, Measurement of $\sin 2\beta$ in $B_d \to J/\psi K_s$(talk) 2 March 1998

[17] Private discussions with Dr.Lednicky

[18] Private discussions with F.Tartarelli

[19] M.Smizanska, Nucl. Phys.B(Proc.Suppl.) 55A(1997) 269-276

[20] M.Smizanska et al., PHYS-NO 041,Nucl. Instrum. Methods A351 (1994) 84-94

[21] P.Eerola et al.,ATLAS Internal Note PHYS-No-054, December 1994

[22] P.Johnson, ATLAS Internal Note PHYS-No-073, October 1995

[23] L.Leinonen, ATLAS Internal Note PHYS-No-082, March 1996

[24] CLEO, Nucl.Instr.Meth.in Phys.Res. A351(1994), page 19

[25] Dunietz et al.,SLAC-PUB-5270, November 1990

[26] Private discussions with J.Schwindling and G.Gonzales

[27] A.R.Edmonds, Angular momentum in quantum mechanics, Princeton university press 1957

[28] D.H.Perkins, Introduction to high energy physics

[29] D.B.Cline, A.Friedman, Annals of The New York Academy of Sciences, Volume 619

[30] P.E.Schlein, Proceedings of the first International Workshop on B-physics at Hadron Machines

[31] M.Guidry, Gauge Field Theories, Oak Ridge, Tennessee

[32] Proceedings of VII International symposium on high energy spin physics, Protvino(USSR) Volume 1, 89-97

[33] ATLAS Technical Proposals, CERN/LHCC/94-43 15 December 1994

[34] ATLAS Inner Detector Technical Design Report,CERN/LHCC/97-16 ATLAS TDR 4, Volumes 1,2

[35] U.Egede, ATLAS Internal Note SOFT-NO-031 15 December 1994

[36] I.Gavrilenko, ATLAS Internal Note INDET-DRAFT 7 January 1996

[37] G.Poulard et al., ATLAS-SOFT/95-draft 15 January 1995

[38] P.Nevski et al., ATLAS-SOFT/95-draft 29 November 1995

[39] F.Luehring, TRT Geometry and Hit Description in DICE95

9 Appendix

i	f_{1i}	f_{2i}	F_i
0	$a_+a_+^* + a_-a_-^* + b_+b_+^* + b_-b_-^*$	1	1
1	$a_+a_+^* - a_-a_-^* + b_+b_+^* - b_-b_-^*$	P_b	$\cos\theta$
2	$a_+a_+^* - a_-a_-^* - b_+b_+^* + b_-b_-^*$	α_Λ	$\cos\theta_1$
3	$a_+a_+^* + a_-a_-^* - b_+b_+^* - b_-b_-^*$	$P_b\alpha_\Lambda$	$\cos\theta\cos\theta_1$
4	$-a_+a_+^* - a_-a_-^* + 1/2b_+b_+^* + 1/2b_-b_-^*$	1	$d^2_{00}(\theta_2)$
5	$-a_+a_+^* + a_-a_-^* + 1/2b_+b_+^* - 1/2b_-b_-^*$	P_b	$d^2_{00}(\theta_2)\cos\theta$
6	$-a_+a_+^* + a_-a_-^* - 1/2b_+b_+^* + 1/2b_-b_-^*$	α_Λ	$d^2_{00}(\theta_2)\cos\theta_1$
7	$-a_+a_+^* - a_-a_-^* - 1/2b_+b_+^* - 1/2b_-b_-^*$	$P_b\alpha_\Lambda$	$d^2_{00}(\theta_2)\cos\theta\cos\theta_1$
8	$-3Re(a_+a_-^*)$	$P_b\alpha_\Lambda$	$\sin\theta\sin\theta_1\sin^2\theta_2\cos\phi_1$
9	$3Im(a_+a_-^*)$	$P_b\alpha_\Lambda$	$\sin\theta\sin\theta_1\sin^2\theta_2\sin\phi_1$
10	$-3/2Re(b_-b_+^*)$	$P_b\alpha_\Lambda$	$\sin\theta\sin\theta_1\sin^2\theta_2\cos(\phi_1+2\phi_2)$
11	$3/2Im(b_-b_+^*)$	$P_b\alpha_\Lambda$	$\sin\theta\sin\theta_1\sin^2\theta_2\sin(\phi_1+2\phi_2)$
12	$-3/\sqrt{2}Re(b_-a_+^* + a_-b_+^*$	$P_b\alpha_\Lambda$	$\sin\theta\cos\theta_1\sin\theta_2\cos\theta_2\cos\phi_2$
13	$3/\sqrt{2}Im(b_-a_+^* + a_-b_+^*$	$P_b\alpha_\Lambda$	$\sin\theta\cos\theta_1\sin\theta_2\cos\theta_2\sin\phi_2$
14	$-3/\sqrt{2}Re(b_-a_-^* + a_+b_+^*$	$P_b\alpha_\Lambda$	$\cos\theta\sin\theta_1\sin\theta_2\cos\theta_2\cos(\phi_1+\phi_2)$
15	$3/\sqrt{2}Im(b_-a_-^* + a_+b_+^*$	$P_b\alpha_\Lambda$	$\cos\theta\sin\theta_1\sin\theta_2\cos\theta_2\sin(\phi_1+\phi_2)$
16	$3/\sqrt{2}Re(a_-b_+^* - b_-a_+^*$	P_b	$\sin\theta\sin\theta_2\cos\theta_2\cos\phi_2$
17	$-3/\sqrt{2}Im(a_-b_+^* - b_-a_+^*$	P_b	$\sin\theta\sin\theta_2\cos\theta_2\sin\phi_2$
18	$3/\sqrt{2}Re(b_-a_-^* - a_+b_+^*$	α_Λ	$\sin\theta\sin\theta_2\cos\theta_2\cos(\phi_1+\phi_2)$
19	$-3/\sqrt{2}Im(b_-a_-^* - a_+b_+^*$	α_Λ	$\sin\theta\sin\theta_2\cos\theta_2\sin(\phi_1+\phi_2)$

Table 8: Definition of functions appearing in Λ_b decay angular distribution(eq.36). For details see [1] and [2].

parameter	**type 1**	**type 2**
events number	10120/year	3200/year
$J/\psi \oplus K_s$		
without cuts	100%(13730/year)	100%(1267/year)
cut 1	3.4%(473/year)	10.8%(136/year)
cuts 1+2	0.8%(104/year)	3.1%(39/year)
cuts 1+2+3	0.5%(72/year)	1.6%(20/year)
cuts 1+2+3+4	0.4%(59/year)	9.5%(162/year)
$J/\psi \oplus K_s \oplus \pi_0$		
with $J/\psi \oplus K_s$ cuts	100%(4900/year)	100%(275585/year)
cut 5	3%(149/year)	3.3%(8914/year)
cuts 5+6	0.08%(4/year)	0.13%(366/year)
cuts 5+6+7	-	0.07%(182/year)
$J/\psi \oplus K_s \oplus \gamma \oplus \gamma$		
with $J/\psi \oplus K_s$ cuts	100%(242116/year)	100%(13335869/year)
cuts 5	4%(9489/year)	4.6%(617867/year)
cuts 5+6	0.4%(1074/year)	0.5%(67195/year)
cuts 5+6+7	0.2%(444/year)	0.2%(27096/year)
cuts 5+6+7+8	0.004%(9/year)	0.01%(1832/year)
cuts 5+6+7+8+9	0.0008%(2/year)	0.008%(1035/year)

Table 9: Information about background. Type 1 and type 2 correspond to background coming from processes $b\bar{b} \to J/\psi\mu X$(Values in third column are valid for process $B_d \to J/\psi K_s$) and $bB_d \to J/\psi K^*(K_0\pi_0)\mu X$(Background events are valid for combinatorial background here). Initial background is set up to 100% and other numbers stand for remaining background level after presented cuts. Numbers in parentheses are numbers of background events produced per one year

parameter	**numerical value**
signal events per year ($\Lambda_b \to J/\psi\Lambda_0$ events with $J/\psi \to \mu^+\mu^-, \quad p_T^\mu > 6GeV, \quad p_T^\mu > 3GeV$ in $\|\eta\| < 2.5$ and $\Lambda_0 \to p\pi$ with $p_T^{\pi,p} > 0.5GeV$ in $\|\eta\| < 2.5$)	$N_s = 2.055 \times 10^5$
PL(particle level) reduction factor (ϵ_{PL} is defined as the ratio of Monte Carlo events with Λ_0 decay radius 1<R<44cm and Λ_b proper time τ_{Λ_b}>0.5 ps to the total number of Monte Carlo events)	$\epsilon_{PL} = 0.351$
overall J/ψ reconstruction efficiency (J/ψ candidate must satisfy:χ^2<20 and mass $\Leftrightarrow 3\sigma(J/\psi) < M < 3\sigma(J/\psi)$	$eff(J/\psi) = 0.901$
overall Λ_0 reconstruction efficiency (Λ candidate must satisfy:χ^2<6 , mass $\Leftrightarrow 3\sigma(\Lambda_0) < M < 3\sigma(\Lambda_0)$ and decay radius 1<R<44 cm)	$eff(\Lambda_0) = 0.559$
overall Λ_b reconstruction efficiency (Λ_b must satisfy:proper time τ_{Λ_b}>0.5 ps, mass $\Leftrightarrow 3\sigma(\Lambda_b) < M < 3\sigma(\Lambda_b)$)	$eff(\Lambda_b) = 0.479$
J/ψ mass resolution	$\sigma(J/\psi) = 39MeV$
Λ_0 mass resolution	$\sigma(\Lambda_0) = 2.5MeV$
Λ_b mass resolution	$\sigma(\Lambda_b) = 22MeV$
Λ_b decay radius resolution	$\sigma(R) = 85\mu m$
Λ_b proper time resolution	$\sigma(\tau) = 0.079ps$
Max.statistical error of P_b	$\delta(P_b) = 0.025$

Table 10: Overall Λ_0,Λ_b and J/ψ fitted parameters